Tectonophysics 637 (2014) 251–267

Contents lists available at ScienceDirect

Tectonophysics

journal homepage: www.elsevier.com/locate/tecto

Crustal structure of the Gulf of Aden southern margin: Evidence from receiver functions on Socotra Island (Yemen)

Abdulhakim Ahmed [a,b,c], Sylvie Leroy [a,b,*], Derek Keir [d], Félicie Korostelev [a,b], Khaled Khanbari [e,f], Frédérique Rolandone [a,b], Graham Stuart [g], Mathias Obrebski [h]

[a] Sorbonne Universités, UPMC Univ Paris 06, UMR 7193, Institut des Sciences de la Terre Paris (iSTeP), F-75005 Paris, France
[b] CNRS/INSU, UMR 7193, Institut des Sciences de la Terre Paris (iSTeP), F-75005 Paris, France
[c] Seismological and Volcanological Observatory Center, Dhamar, Yemen
[d] National Oceanography Centre Southampton, University of Southampton, Southampton, SO14 3ZH, UK
[e] Yemen Remote Sensing Center and Department of Earth and Environmental Science, Sana'a University, Yemen
[f] Sana'a University, Yemen
[g] School of Earth and Environment, University of Leeds, Leeds, UK
[h] Lamont-Doherty Earth Observatory, University of Columbia, NY, USA

ARTICLE INFO

Article history:
Received 22 March 2014
Received in revised form 23 September 2014
Accepted 13 October 2014
Available online 27 October 2014

Keywords:
Magma-poor margin
Crustal deformation
Margin segmentation
Necking zone
Gulf of Aden
Receiver function

ABSTRACT

Breakup of continents in magma-poor setting occurs primarily by faulting and plate thinning. Spatial and temporal variations in these processes can be influenced by the pre-rift basement structure as well as by early syn-rift segmentation of the rift. In order to better understand crustal deformation and influence of pre-rift architecture on breakup we use receiver functions from teleseismic recordings from Socotra which is part of the subaerial Oligo-Miocene age southern margin of the Gulf of Aden. We determine variations in crustal thickness and elastic properties, from which we interpret the degree of extension related thinning and crustal composition. Our computed receiver functions show an average crustal thickness of ~28 km for central Socotra, which decreases westward along the margin to an average of ~21 km. In addition, the crust thins with proximity to the continent–ocean transition to ~16 km in the northwest. Assuming an initial pre-rift crustal thickness of 35 km (undeformed Arabian plate), we estimate a stretching factor in the range of ~2.1–2.4 beneath Socotra. Our results show considerable differences between the crustal structure of Socotra's eastern and western sides on either side of the Hadibo transfer zone; the east displays a clear intracrustal conversion phase and thick crust when compared with the western part. The majority of measurements across Socotra show V_p/V_s ratios of between 1.70 and 1.77 and are broadly consistent with the V_p/V_s values expected from the granitic and carbonate rock type exposed at the surface. Our results strongly suggest that intrusion of mafic rock is absent or minimal, providing evidence that mechanical thinning accommodated the majority of crustal extension. From our observations we interpret that the western part of Socotra corresponds to the necking zone of a classic magma-poor continental margin, while the eastern part corresponds to the proximal domain.

1. Introduction

The eastern Gulf of Aden continental margins are magma-poor oblique-rifted margins (Fig. 1a) (Bellahsen et al, 2013a; Leroy et al, 2010a). As such, long fracture zones generated by transform faults impose a first order control on the along-rift segmentation of the young ocean basin (Bellahsen et al, 2013b; Leroy et al., 2012). The Arabian plate is thought to have broken away from the Somalian plate at 20–18 Ma, with the young passive rifted conjugate margins still largely exposed subaerially (d'Acremont et al., 2010; Fournier et al., 2010). This makes it easy to interpret the extensional and sedimentary processes active during continental breakup. Post-rift sedimentary cover is generally relatively thin (0.5–1 km) (d'Acremont et al., 2005; Leroy et al., 2004) and seismic reflection profiles show an absence of seaward dipping reflectors (Autin et al., 2010a,b; d'Acremont et al., 2005; Leroy et al., 2010a,b) making syn/post-rift sediment and basement easily identifiable and mappeable. The structure of the margin is therefore interpretable on upper-crustal and crustal scale cross sections (Autin et al., 2010a; d'Acremont et al., 2005, 2006, 2010; Leroy et al., 2004, 2010a, 2012; Tiberi et al., 2007).

Magma-poor rifted margins show a characteristic architecture within three distinct divisions from continent to ocean: the proximal, distal, and ocean-continent transition domains. The proximal domain is characterized by rift-basins bound by high-angle listric faults with

* Corresponding author at: CNRS/INSU, UMR 7193, Institut des Sciences de la Terre Paris (iSTeP), F-75005 Paris, France. Tel.: +33 144273408; fax: +33 144274950.
E-mail address: sylvie.leroy@upmc.fr (S. Leroy).

http://dx.doi.org/10.1016/j.tecto.2014.10.014
0040-1951/

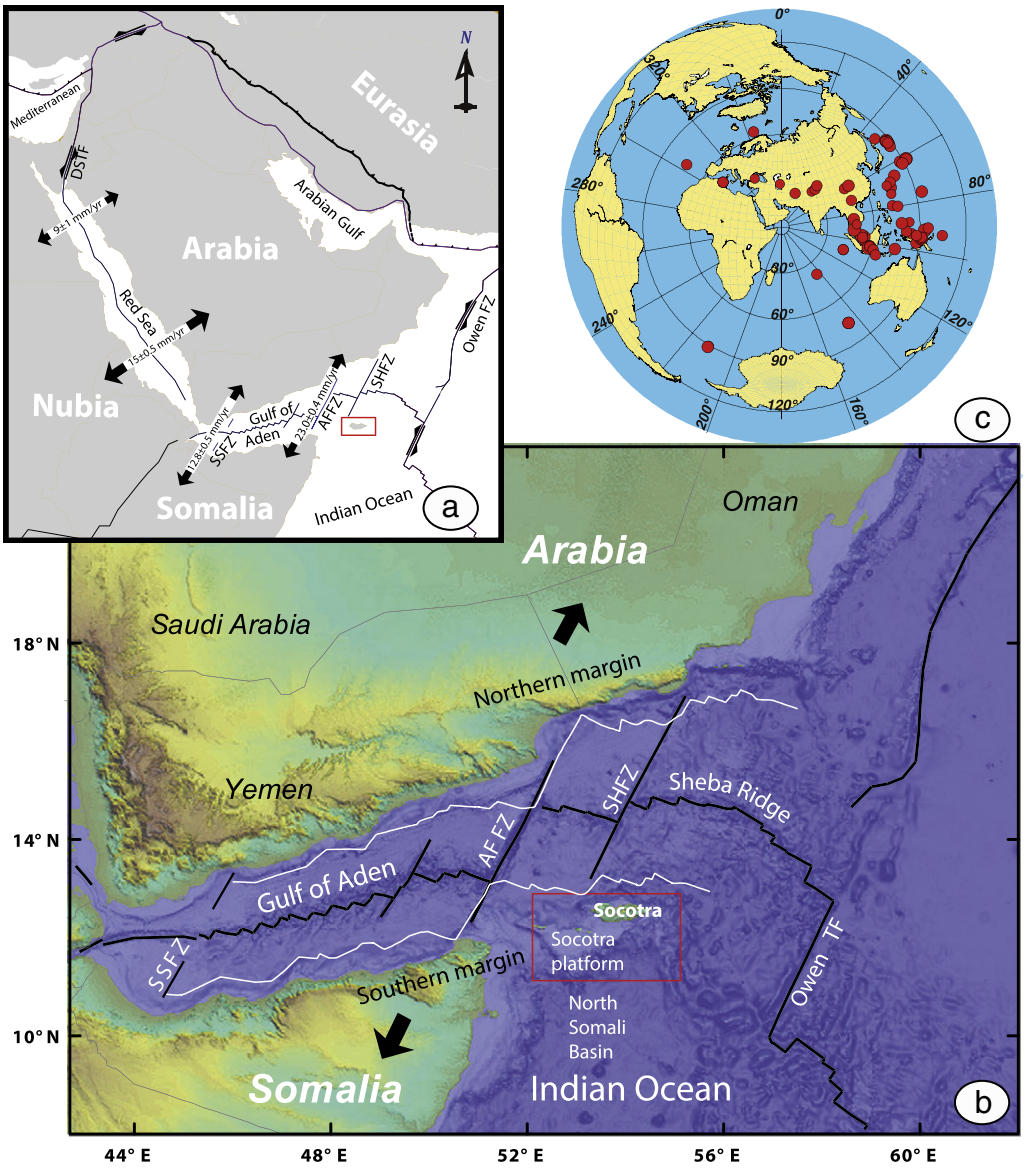

Fig. 1. a) and b) Landsat imagery and Sea-sat bathymetry showing the main tectonic features of the Gulf of Aden and surrounding areas. The large black arrows indicate the direction of plate motion in the region. The white lines show the location of the first magnetic anomaly (5d = 17.6 Ma) identified in the Gulf of Aden (d'Acremont et al., 2006; Leroy et al., 2010a, 2012). c) Polar projection shows the distribution of seismic events, small circle interval is 30°. SSFZ: Shukra el Sheik fracture zone; AFFZ: Alula Fartak fracture zone; SHFZ: Socotra Hadbeen fracture zone; DSTF: Dead Sea transform fault, Owen TF: Owen transform fault.

limited crustal thinning ($\beta < 2$) (e.g. Mohn et al., 2012). The crust of the distal domain is extremely thin with listric detachment faults commonly penetrating the whole crust. This differs from the proximal domain where fault does not cut through the whole crust (Franke, 2013; Péron-Pinvidic and Manatschal, 2008; Whitmarsh et al., 2001). Mohn et al. (2012) defined a narrow necking zone between proximal and distal domains. Necking of the continental crust occurs in a narrow transition zone from slightly stretched and thinned crust (~30 km) to extremely thinned crust (<10 km) with $\beta > 2$ (Mohn et al., 2012). The ocean-continent transition (OCT) is defined as the domain of exhumed sub-continental mantle (Franke, 2013; Mohn et al., 2012) if it has been sampled. If no samples are available then the OCT is defined as a domain of uncertain affinity between the thinned continental crust and the crust that displays clear oceanic geophysical characteristics (see Leroy et al., 2010a for details). Hence, crustal thickness variation along rifted margins from the proximal domain to the distal domain is a key parameter required to assess structural segmentation and the strain localization during the transition from continental break-up to active oceanic spreading.

During the last few decades, detailed geophysical and geological studies have been carried out within the Gulf of Aden to evaluate the initiation and development of the active spreading ridge (Sheba ridge) (Fig. 1a and b). These studies have provided bathymetric (Leroy et al., 2004), seismic (Autin et al., 2010a; Bache et al, 2011; d'Acremont et al., 2005, 2010; Laughton et al., 1970; Leroy et al., 2004, 2010a,b; Stein and Cochran, 1985; Watremez et al., 2011), gravity, magnetic (Ali and Watts, 2013; d'Acremont et al., 2006; Fournier et al., 2010; Leroy et al., 2010a; Leroy et al, 2012), and heat flow (Lucazeau et al., 2008, 2009, 2010; Rolandone et al, 2013) constraints. The interpretation of these data has resulted in a detailed model of the evolution of the eastern Gulf of Aden from rifting to oceanic spreading. In addition to these marine geophysical studies, detailed onshore stratigraphical, geological, structural, and geophysical studies have been carried out on the northern continental margin of the Gulf in eastern Yemen and Oman (Ahmed et al, 2013; Al- Hashmi et al., 2011; Al-Lazki et al., 2012; Basuyau et al., 2010; Bellahsen et al., 2006, 2013a,b; Chang and Van der Lee, 2011; Corbeau et al, 2014; Denèle et al, 2012; Huchon and Khanbari, 2003; Korostelev et al, 2014; Leroy et al., 2012; Menzies

et al., 1992, 1997; Platel and Roger, 1989; Platel et al., 1992; Robinet et al., 2013; Tiberi et al., 2007). These studies reveal extension directions of N20°E parallel to the plate motion and N160°E perpendicular to the main direction of the oblique rift (Autin et al., 2010b; Brune and Autin, 2013) and thinning of the crust from a thickness of 35 km at 30 km inland from the coast to a thickness of 26 km at the coast. Unfortunately, it has not been possible to carry out similar studies along the southern margin of the Gulf of Aden, where the surface geology investigation was previously limited to field mapping of the Socotra archipelago (e.g., Beydoun and Bichan, 1969; Samuel et al., 1997; Fournier et al., 2007; Leroy et al., 2012; Denèle et al., 2012; Bellahsen et al., 2013b; Pik et al., 2013), a shallow marine seismic reflection line on the southern Socotra platform (Birse et al., 1997; Morrison et al., 1997) and field mapping in Somalia (e.g., Brown, 1931; Fantozzi, 1996; Fantozzi and Sgavetti, 1998; Granath, 2001). Socotra island constitutes an important part of the southern margin located at the easternmost part of the Gulf of Aden (Fig. 1b). It documents the full geological and tectonic history of rifting, including a record of the pre-rift continental architecture that existed when it was still attached to Arabia, as well as the complex geological and tectonic syn-rift stage and post-rift geological and tectonic processes (Leroy et al., 2012). These previous studies do not include imaging of the deep crustal structure that is critical to evaluate crustal scale deformation history and evolution during rifting.

With this purpose in mind, the Socotra component of the YOCMAL (Young Conjugate Margins Laboratory) seismic project was conceived and implemented during 2010–2012. YOCMAL deployed 24 new broadband seismic stations to supplement the single permanent seismic station to provide data coverage for the entire island of Socotra. We use teleseismic waveform data from our network to quantify for the first time the variation of the crustal thickness and elastic properties of Socotra. This study provides data and interpretation on the evolution of the whole crust of the southern Aden margin. This enables an interpretation of the breakup history in the context of the better-known northern conjugate margin in Oman, leading to an understanding of rift evolution. We use our results beneath Socotra to better understand plate scale deformation and compositional modification thus improving our understanding of the breakup history of the youngest non-volcanic passive continental margin on Earth.

2. Geological and tectonic setting

Socotra is the largest of four islands (Socotra, Darsah, Samhah and Abd al Kuri) constituting the Socotra Archipelago located east of Somalia and representing the southeastern Gulf of Aden margin. Geographically Socotra is ~380 km south of Ras Fartaq in mainland Yemen and ~250 km east of the Horn of Africa (Fig. 1).

The greatest depth to the seafloor surrounding the islands is ~2500 m, north of the archipelago. The ~70 km wide Socotra Platform to the south of the islands is at water depths of less than ~250 m. South of the Socotra Platform the seafloor drops to ~5000 m in the North Somali Basin (Birse et al., 1997) (Fig. 1).

The continental rifting which eventually formed the Gulf of Aden conjugate margins began as early as the Oligocene (~34 Ma) with the formation of rift valley grabens (d'Acremont et al., 2005, 2006, 2010; Leroy et al., 2010a, 2012; Robinet et al., 2013). Beginning in the early Miocene (~17.6 Ma), oblique seafloor spreading with a mean extension direction of N20°E began to separate the two N75°E trending conjugate margins (Leroy et al., 2004; Bellahsen et al. 2006; d'Acremont et al., 2006, 2010; Leroy et al., 2010a, 2012) (Fig. 1). Continental breakup resulted in distinct eastern and western structural domains of Socotra, separated by the NE-SW striking Hadibo transfer zone (HTZ) located through the middle of the island (Fig. 2; Beydoun and Bichan, 1969; Leroy et al., 2012; Bellahsen et al., 2013b). The eastern domain is composed of a single large tilted block dominated by igneous rocks which forms the ~1500 m high Haggier Mountain Range. The western domain is characterized by tilted blocks bound by ~N110°E trending faults (Bellahsen et al., 2013b; Leroy et al., 2012).

The pre-rift geology of Socotra is a neoproterozoic basement and Cretaceous-Eocene carbonates. The Neoproterozoic basement, which is composed of metamorphic, plutonic and volcanic rocks (Denèle et al., 2012), outcrops over more than 30% of the eastern domain in the Haggier Mountains (Fig. 2). In the western domain, basement consisting mainly of metamorphic and biotite granite rocks outcrops at Qalansiya and Sherubrub (Fig. 2). Pre-rift carbonate-dominated Cretaceous strata were deposited uncomformably over the basement, followed by Paleocene/Middle Eocene carbonate shelf deposits (Beydoun and Bichan, 1969; Leroy et al., 2012).

The pre-rift strata were disturbed by the onset of rifting in the early Oligocene, with the regional stratigraphy providing age constraints on the rift history (Leroy et al., 2012). Syn-rift carbonate sediments were deposited in three fault bound Oligocene basins preserved in the western domain of the island (Fig. 2). Of these the Allan–Kadama and Sherubrub–Balan basins are bound by ~N110°E trending low-angle normal faults, and the Central Basin is aligned with the southern part of the HTZ (Bellahsen et al., 2013b) (Fig. 2). The HTZ is a pre-existing structure associated with Permian–Triassic rifting which was reactivated during the opening of the Gulf of Aden (Bellahsen et al., 2013b; Denèle et al., 2012; Leroy et al., 2012). There are no syn-rift sediments on the eastern domain and the spatially limited rift faults are high angle (e.g. in Jebel Haggier) (Fig. 2).

Recent thermochronological dating indicates a slightly younger age of rift development in the eastern Socotra domain (38 ± 2 Ma) compared to the western Socotra domain (32 ± 2 Ma), which suggests that the HTZ was already reactivated at that time (Pik et al., 2013). A second phase of uplift and erosion is recorded only in the strata of the eastern part of the island at 20 ± 2 Ma. This post-dates the onset of rifting, but is synchronous with development of the OCT offshore (Leroy et al., 2010a; Pik et al., 2013). The maximum denudation is close to the HTZ.

Post-rift sediments sealed the rifted-blocks faults activity with dominant vertical movement from the end of the Miocene to the Quaternary. This resulted in deposition of deltaic fans of continent-derived conglomerates in local basins during a major uplift phase (Leroy et al., 2012). This was followed by subsidence and marine deposition on eroded, older pre-rift and syn-rift strata (Beydoun and Bichan, 1969; Leroy et al., 2012).

3. Data and methodology

3.1. Data

A temporary seismic network of 24 three-component broadband stations in total was installed on Socotra. The network operated for a period of 12 months in two time periods between March 2010 and March 2011 and September 2011 to September 2012 as part of the YOCMAL seismic project. The seismic stations were distributed over the entire island of Socotra with station separation ranging from 5 to 40 km (Fig. 2). Firstly, the seismic network consisted of 6 Güralp CMG-3ESPD (60 s natural period) sensors, 13 Güralp CMG-6TD (30 s natural period) sensors and 2 Güralp CMG-40T (30 s natural period) sensors with RefTek-130 data acquisition systems. Additional data were collected from 3 temporary broadband stations (Fig. 2) equipped with Güralp CMG-40T sensors and RefTek-130 data acquisition systems, operated as an auxiliary part of the YOCMAL seismic project for 12 months between September 2011 and September 2012. In addition, data from one permanent GFZ broadband station SOCY, which was equipped with an STS-2 seismometer and a Quanterra-330 datalogger (shown as triangle in Fig. 2), were analyzed.

The seismic data were continuously sampled at 40 Hz by the temporary seismic stations and at both 100 and 20 Hz by the permanent

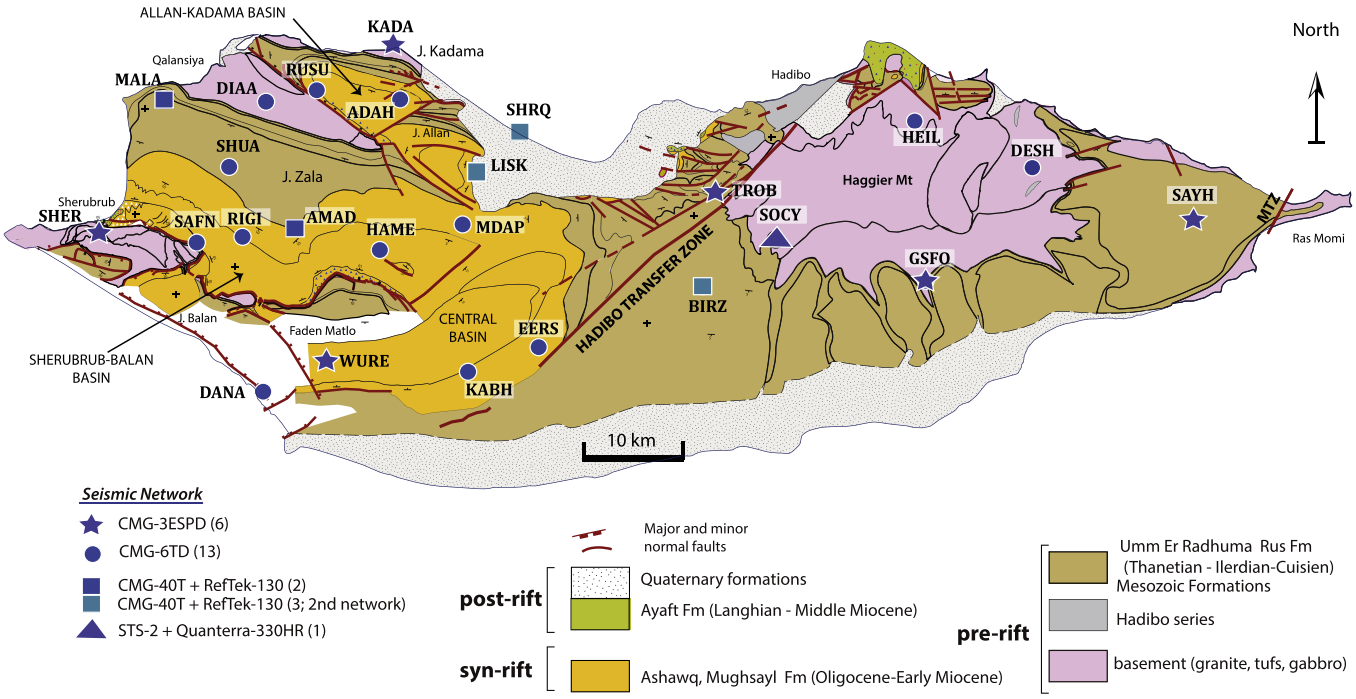

Fig. 2. Geological map of the study area showing geological units (modified from Leroy et al., 2012; Denele et al., 2012), location of YOCMAL temporary network of 24 seismic stations on Socotra and SOCY station, one of the Yemen-GFZ permanent seismic network.

network. All stations were equipped with GPS timing systems operated in continuous mode to synchronize the stations' internal clocks.

We used 100 teleseismic events with magnitudes >5.5 within an epicentral distance range of 25°–95° from each station (Fig. 1c). The raw waveform data were windowed to start 30 s before and ending 30 s after the computed IASP91 P-arrival time. We filtered the selected signal with a zero phase Butterworth bandpass filter with corner frequencies of 0.05–0.8 Hz. Based on the signal-to-noise ratio of P-wave phase and disturbances (e.g., spikes, glitches, sensor re-centering, calibration pulses, missing data…etc.) within 30 s after the P-wave arrival, we selected the best waveform data recorded at each station. The signal-to-noise ratio of P-wave phase is calculated using SN = A_s/A_n, where A_s is the signal root mean square variance in the time window of 2 s before and 18 s after the P-arrival time, and A_n is the noise root mean square variance in the time window of 22 s–2 s before the P-arrival time. Events with a signal to noise ratio (SN) of three or greater on the vertical component were selected and converted to radial and tangential RFs (Ligorria and Ammon, 1999).

Table 1
Crustal thickness (H) and V_p/V_s ratio results for seismic stations on Socotra. The average crustal velocity used is 6.4 km/s. The average crustal velocity is based on previous studies of the velocity structure for the Arabian platform (e.g., Al-Amri, 1998, 1999; Mooney et al., 1985).

Station name	Number of RF	Latitude (N)	Longitude (E)	Elevation (m)	Crustal thickness (H, km)	V_p/V_s ratio	Error in depth (km)	Error in V_p/V_s
ADAH	44	12.6513	53.6509	217	21.6	1.77	0.83	0.033
AMAD	27	12.5072	53.5747	134	23.2	1.84	0.43	0.029
BIRZ	20	12.4786	53.9209	882	30.2	1.73	1.1	0.027
DANA	35	12.3907	53.5230	251	26.6	1.80	0.66	0.038
DESH	29	12.5830	54.2392	89	23.6	1.77	1.08	0.034
DIAA	41	12.6509	53.5299	76	19.6	1.65	0.39	0.016
EERS	18	12.4269	53.7719	151	28.2	1.73	2.11	0.055
GSFO	56	12.4774	54.1399	134	27.6	1.78	0.74	0.026
HAME	32	12.5166	53.6305	124	20.2	1.76	0.47	0.023
HEIL	28	12.6266	54.1296	87	28.6	1.70	0.99	0.032
KABH	36	12.4059	53.7080	137	26.8	1.76	0.33	0.017
KADA	45	12.6993	53.6449	35	16.8	1.89	0.59	0.037
LISK	23	12.5840	53.7185	44	22.0	1.77	0.48	0.045
MALA	38	12.6550	53.4380	680	21.4	1.71	0.61	0.052
MDAP	23	12.5382	53.7054	52	23.4	1.77	0.52	0.031
RIGI	38	12.5304	53.5067	239	23.0	1.77	1.07	0.043
RUSU	25	12.6605	53.5755	100	16.4	1.71	1.69	0.054
SAFN	34	12.5261	53.4649	156	23.4	1.73	0.63	0.048
SAYH	34	12.5340	54.3903	360	22.4	1.82	0.6	0.044
SHER	20	12.5356	53.3777	41	22.2	1.70	1.04	0.046
SHRQ	26	12.6196	53.7583	16	20.0	1.80	1.17	0.058
SHUA	39	12.5932	53.4957	691	21.2	1.83	0.32	0.021
SOCY	30	12.5195	53.9874	804	28.4	1.78	0.213	0.012
TROB	55	12.5630	53.9327	150	28.2	1.94	1.39	0.043
WURE	56	12.4176	53.5806	179	26.4	1.73	0.39	0.032

The RFs then evaluated with careful visual inspection to accept those with a clear positive polarity P-wave arrival at, or shortly after zero time on the radial signal. In addition, accepted RFs have a tangential signal with smaller amplitudes compared to the radial signal and have no significant ringing on the radial or tangential signals.

The number of events used for final analysis at each station varies from 18 to 56 (Table 1), depending on the background noise and the technical state of the station. Most of the selected events have an ENE backazimuth with some events from the south and some from the northwest (Fig. 1c).

3.2. Receiver function analysis

The receiver function method maps the seismic discontinuities within the Earth below three-component seismic stations by removing the effects of the source, propagation path and instrument response from the waveform of incident teleseismic P-waves that have been partially converted to S-waves. The amplitudes and polarity of the converted phases are sensitive to the impedance contrasts between the layers above and below the seismic discontinuity. The delayed arrival time of the P-waves converted to S-waves compared to the arrival time of the direct P-wave is a function of P- and S-waves velocities above the seismic discontinuity and the depth of the discontinuity (Fig. 3f). Hence, crustal thickness and elastic property information can be derived from receiver function analysis (0wens et al., 1984; Langston, 1977, 1979; Vinnik, 1977; Zandt et al., 1995).

We employ the iterative time domain deconvolution technique developed by Ligorria and Ammon (1999) to compute the receiver functions. We calculate the receiver function by applying several processing steps. The N-S and E-W horizontal components were rotated to radial and tangential components. A 30 s time window (5 s before the theoretical P arrival time and 25 s after) was used to deconvolve the vertical component from the radial and transverse components. We applied a Gaussian filter of 2.5 to the deconvolved spike wave train, except for the noisiest stations where a Gaussian width of 2.0 is used to smooth the receiver function (e.g., Ligorria and Ammon, 1999). Fig. (4) and Fig. (S1) show the individual RFs at each station plotted as a function of backazimuth, and Fig. (3a–d) shows the stacked receiver functions for all stations.

We adopt the H–k domain stacking technique (Zhu and Kanamori, 2000), to estimate the crustal thickness (H) and the average crustal V_p/V_s ratio (k). Inversion results can be seen in Fig. 5 and Fig. S2. The method sums the receiver function amplitudes of the Moho conversion of P- to S-waves and its multiple converted phases (PpPs and PpSs + PsPs) (Fig. 3f) at predicted arrival times for different crustal thickness (H) and V_p/V_s ratio (k) pairs, transforming them from time

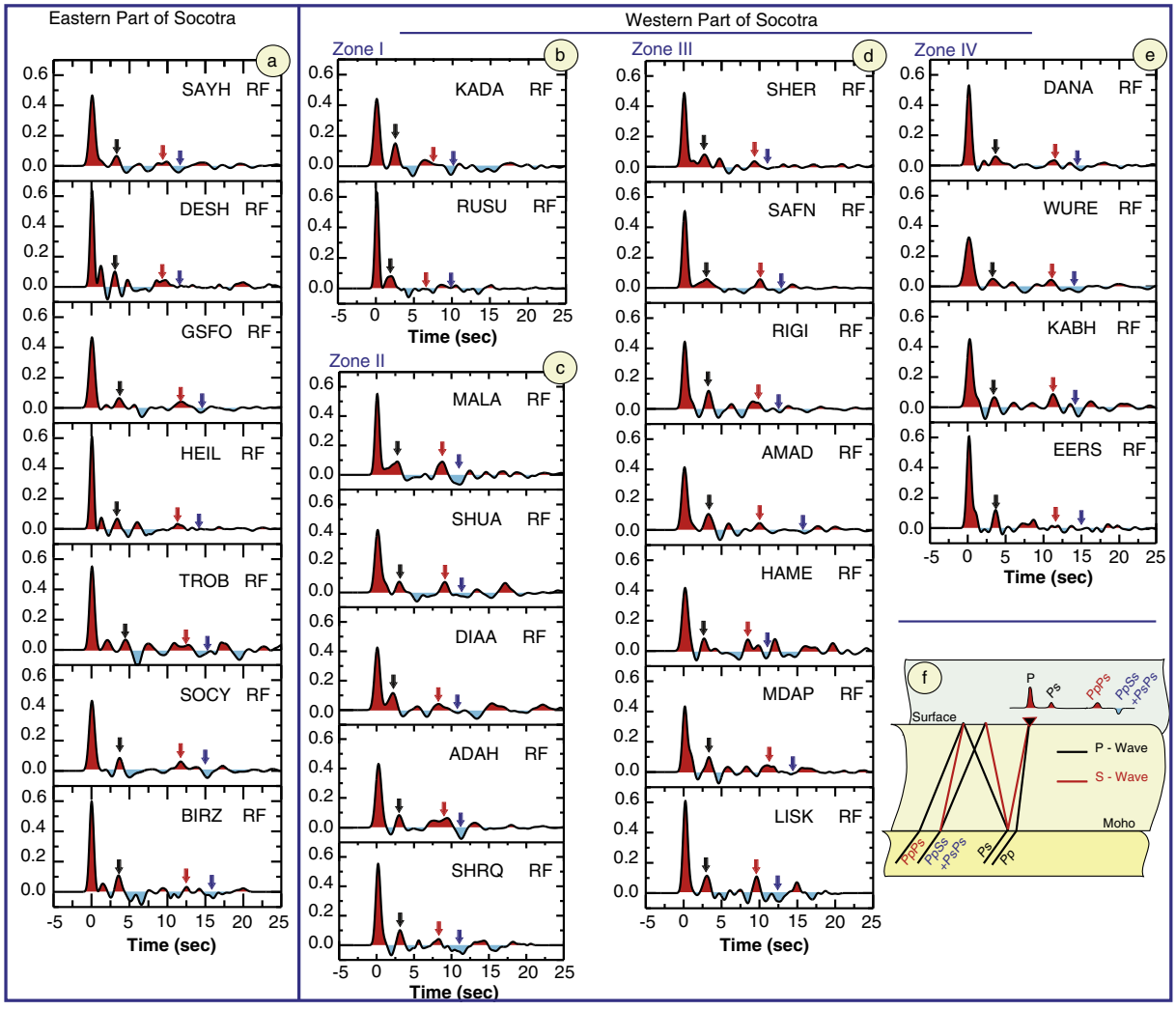

Fig. 3. Stacked receiver functions for the 24 seismic stations of the ANR-YOCMAL network and one permanent station on Socotra: a) for the eastern domain of Socotra, b–e) for the western domain of Socotra. The arrows represent the arrival of the Moho Pms (black), PpPs (red) and PpSs + PsPs (blue) phases from the Moho. See inset in f) for explanation of the Moho Pms and the multiple phase crustal paths.

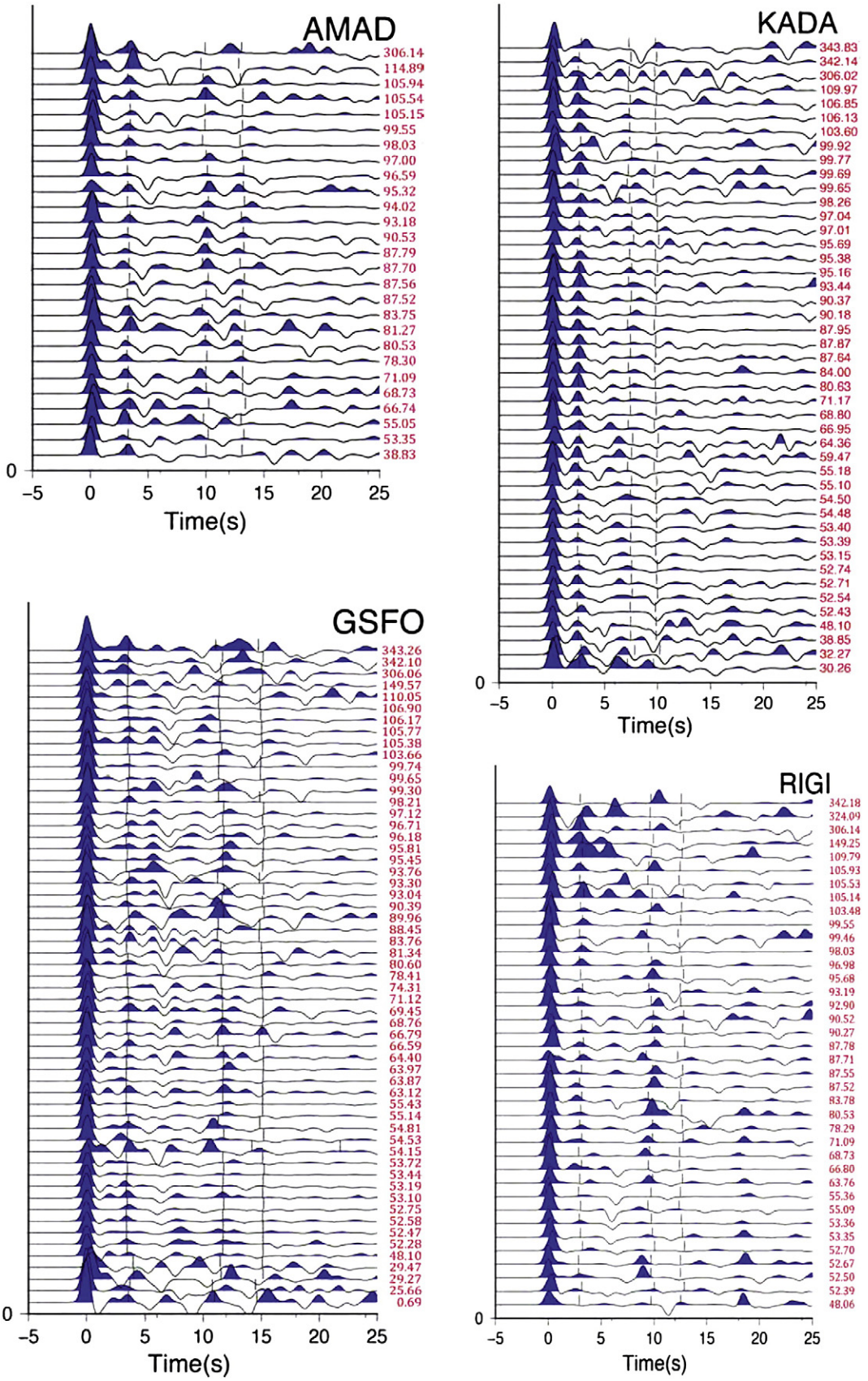

Fig. 4. Individual receiver functions for 4 stations on Socotra. The receiver functions are organized by increasing backazimuth (red number right of the trace). The light vertical lines indicate arrival times for conversion phases (Pms and multiples) from the Moho for the maximum stacking amplitude.

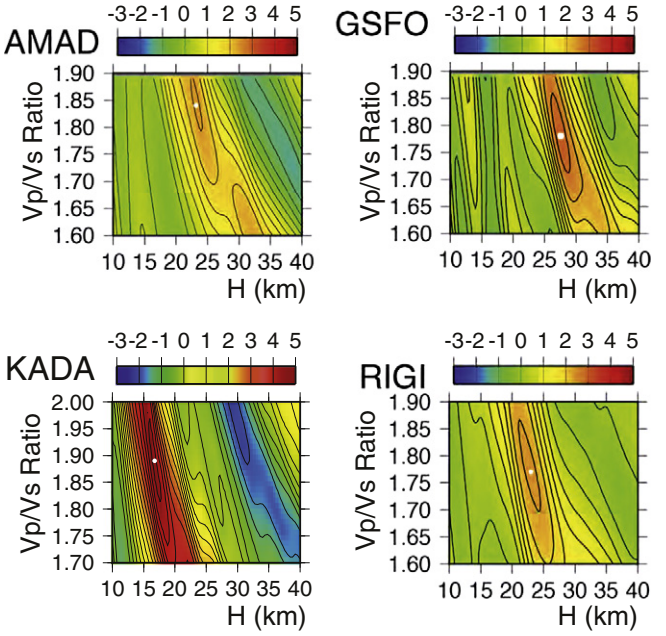

Fig. 5. Thickness (H) versus V_p/V_s ratio diagrams from the H–k stacking method for the 4 stations presented in Fig. 4. The maximum stacking amplitude is indicated by the white point and corresponds to the value indicated in Table 1. The scale bar is the amplitude of stacking function.

domain to H–k domain. This approach assumes an average V_p for the whole crust and the best estimate for the crustal model is achieved with the maximum summation:

$$s(H,k)=\sum_{i=1}^{n}\left[w_1 r_i(t_{\mathrm{Pms}})+w_2 r_i\left(t_{\mathrm{PpPs}}\right)-w_3 r_i\left(t_{\mathrm{PpSs+PsPs}}\right)\right] \quad (1)$$

where n is the number of receiver functions, Wj, (j = 1,2,3) is a weighting factor that represents the contribution of the corresponding seismic phase according to signal-to-noise ratio (with the constraint that W1 + W2 + W3 = 1) and $r_i(t)$ is the amplitude of the receiver function at time t of the associated seismic phase. The primary conversion phase that has the highest signal-to-noise ratio is associated with the highest weight. Low weights (W2 + W3 < W1) are assigned to the multiples (PpPs and PpSs + PsPs) in comparison to the primary phase Pms because the slopes of crustal multiples are very similar in the H–k plane (Zhu and Kanamori, 2000). In case of low signal-to-noise ratio the multiples are down weighted because they are often weak signals and masked by noise. Different values have been tested to evaluate the sensitivity of stacking results to the assigned weight. Then we assign weights of W1 = 0.6, W2 = 0.3 and W3 = 0.1 for the primary phase and multiples, respectively (Zhu and Kanamori, 2000). At a few stations these values have been adjusted based on the visibility of the multiples, using to set of weights W1 = 0.7, W2 = 0.2, W3 = 0.1 and W1 = 0.8, W2 = 0.2, W3 = 0.0.

The theoretical travel times of Pms, PpPs and PpSs + PsPs can be calculated as follows:

$$t_{\mathrm{Pms}}=H\left[\sqrt{(V_s^2-p^2)}-\sqrt{\left(V_p^2-p^2\right)}\right] \quad (2)$$

$$t_{\mathrm{PpPs}}=H\left[\sqrt{(V_s^2-p^2)}+\sqrt{\left(V_p^2-p^2\right)}\right] \quad (3)$$

$$t_{\mathrm{PpSs+PsPs}}=H\left[\sqrt{(V_s^2-p^2)}-\sqrt{\left(V_p^2-p^2\right)}\right] \quad (4)$$

Due to the lack of a-priori velocity information, we tested the H–k technique with a range of average crustal velocities V_p (5.8, 6.0, 6.2, 6.4, 6.6 and 6.8 km/s) to determine the most appropriate average velocity to be used in the inversion for H and k in the different regions of Socotra (an example of the results is shown in the supplementary materials, Fig. S4). We chose a value of 6.4 km/s for average crustal velocity (V_p), in agreement with the global average for continental crust (Christensen and Mooney, 1995) and previous receiver function results in the northern margin of the Gulf of Aden (Ahmed et al., 2013; Tiberi et al., 2007).

A grid search in the 10–40 km interval Moho depth (H) versus 1.6 to 1.9 V_p/V_s ratio (k) is carried out to obtain the maximum stacked amplitude. In the minority of cases, we further limit the searched range of V_p/V_s ratios to avoid unrealistic crustal thickness and/or V_p/V_s results due to some crustal reverberations in the receiver function signal. We show the range of searched k values appear in the H–k diagrams.

We use the bootstrap resampling technique (Efron and Tibshirani, 1986) to estimate the errors of Moho depth and V_p/V_s ratio. The technique randomly samples subsets of receiver functions available for each station, recalculating the Moho depth and V_p/V_s ratio using the Zhu and Kanamori (2000) stacking method. This resampling is repeated 200 times and the standard deviation of these 200 results gives the error estimates for the stacking method and is displayed as error bars in the depth sections. We also use a bootstrap analysis to estimate the errors due to the sensitivity of the method to the assumed V_p value. For each station, we recalculate H and V_p/V_s for 200 randomly chosen values of V_p within the range 5.8 km^{-1} to 6.8 km^{-1} (Tiberi et al., 2007). Results of error estimates are shown in the supplementary material (Fig. S4).

To determine the velocity model of a layered crust that matches our RF results at selected sites of eastern and western domains of Socotra, we perform RF inversion with a stochastic method (Shibutani et al., 1996). The stacked radial receiver functions of each station are inverted for 1-D shear wave velocity structure using the Neighborhood Algorithm (NA) technique (Sambridge, 1999a,b). The initial model is based on the results of previous geophysical studies of the crustal structure beneath the Arabian plate on the northern conjugate margin (e.g., Al-Amri, 1998, 1999; Mooney et al., 1985), and the V_p/V_s ratio is estimated from H–k stacking results. The model parameters are the thickness of the layer, the shear wave velocity at the top and bottom of each layer, the V_p/V_s ratio and the density. Our starting model is composed of 4 to 5 layers: sediment layer when needed, basement, upper crust, lower crust and uppermost mantle. Shear wave velocity construction at each layer and the computation of the synthetic waveforms follow the method implemented by Shibutani et al. (1996).

4. Results

Moho depth H and V_p/V_s results from receiver functions analysis are shown on the geological map of Socotra island Fig. (6a) and (b) respectively. The Pms Moho conversion phase appears clearly at all the stations from individual and stacked receiver functions (Figs. 3 and 4). Multiples (PpPs + PsSs) are clearly observed in the majority of stacked receiver functions; however, the Moho multiples may be disturbed by multiples from intracrustal and/or upper mantle interfaces at some stations (Fig. 4). Calculated crustal thickness and V_p/V_s ratio with uncertainties are compiled in Table 1. We organize the results into the eastern and western domains separated by the HTZ, on the basis of their differing geology and also in light of contrasting crustal properties found in our new study (Fig. 2). Most of the stations in the eastern domain display a clear intracrustal conversion phase and thick crust, contrasting the western domain which has thin crust and the absence of strong intracrustal discontinuities.

4.1. Eastern Socotra

With the exception of SAYH station, clear positive intracrustal phases are observed within 1.23–1.82 s of the direct P-wave arrival.

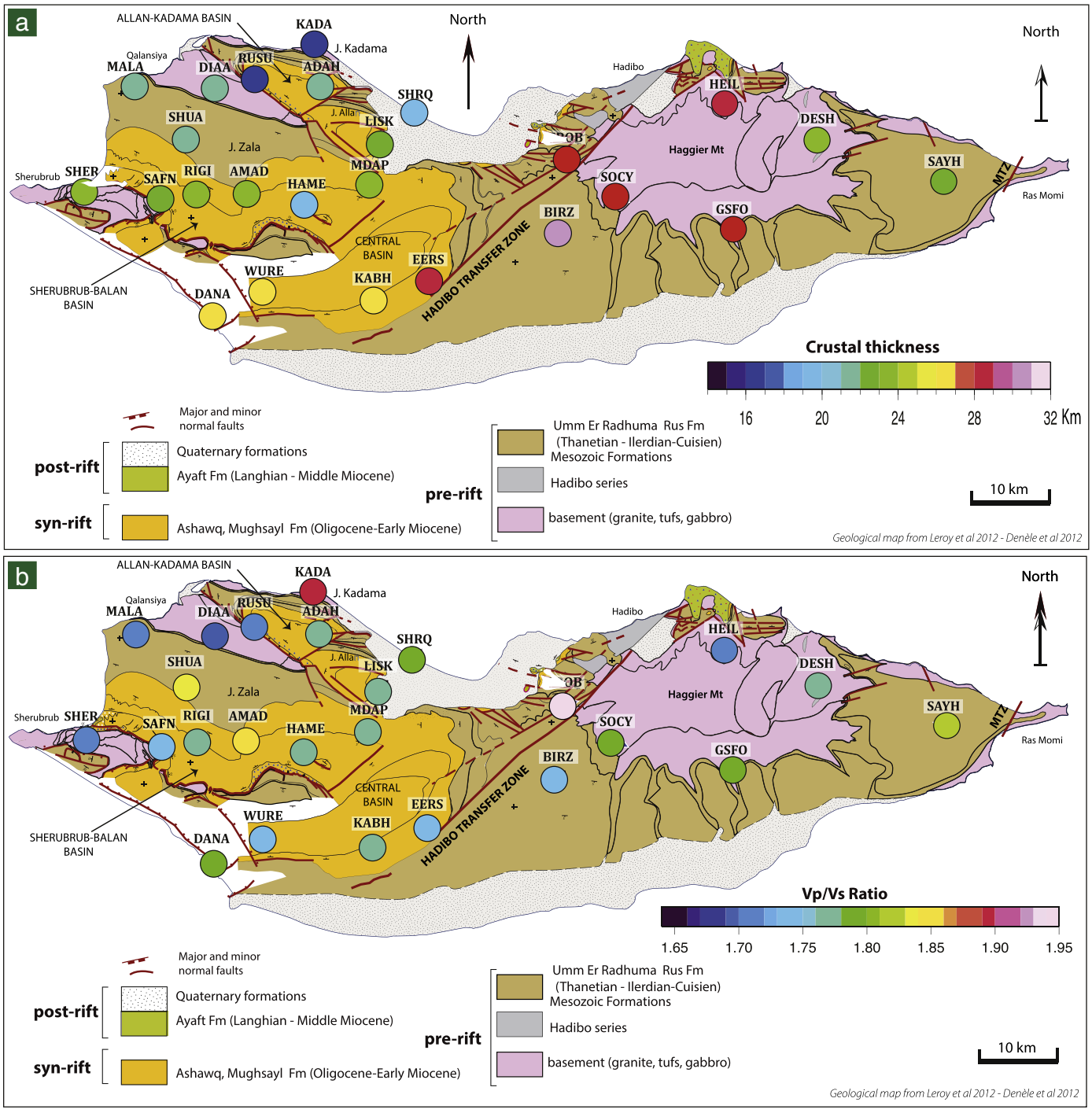

Fig. 6. Maps of crustal thicknesses (H) and V_p/V_s ratios calculated using the H–k method and average crustal velocity of 6.4 km/s. a) Geological map with the crustal thickness variations of Socotra and b) Geological map with the V_p/V_s ratio variations of Socotra.

At some stations (e.g., DESH, HEIL and GSFO) these phases are associated with crustal multiples (PpPs + PsSs) within 5–10 s after the direct P-wave arrival. In all the individual (Fig. 4) as well as stacked receiver functions from all the eastern stations (Fig. 3), a strong positive conversion phase arrives within a delay time of 3.1–3.8 s after the P-wave arrival. These conversions indicate a seismic velocity discontinuity that increases with depth and is interpreted as the Moho discontinuity.

The H–k stacking results (Fig. 6a and b) indicate that the crustal thickness beneath eastern stations increases westward from 22.4 ± 0.6 km (SAYH) to its maximum value of 30.2 ± 1.1 km beneath BIRZ station on the plateau near the HTZ (Fig. 2). The associated V_p/V_s values for the eastern stations range from 1.70 (HEIL) located on the basement rock east of Hadibo to 1.82 (SAYH) located on sedimentary rock at the eastern part of the island. A very high value of 1.94 is estimated for TROB located near HTZ at the northern base of Haggier Mountain (Fig. 6b). The positive phase that arrives before the Moho conversion phase can be attributed to an intracrustal discontinuity located at a depth range of 10–16 km depending on the selected average velocity.

4.2. Western Socotra Island

The crustal thickness of the western domain of the island increases from the NNW to SSE, such that the western part can be divided into EW-trending zones with uniform crustal thickness. These zones broadly correlate with the three Oligocene basins (from north to south being the Allan- Kadama, Sherubrub–Balan, and Central basins). The northernmost zone, located on the northwest coast of the island, is narrow with a Moho Pms conversion phase of 2 to 2.5 s after the first P-wave arrival and multiples within a 7–10.5 s delay (Figs. 2 and 3). The corresponding crustal thickness in this zone is estimated at 16.4 km (RUSU) and 16.8 km (KADA) (Fig. 5 and S1–2). To the south in and around the Sherubrub–Balan basin five stations are characterized by a clear Moho conversion phase that arrives with a delay of 2.3–3.1 s after the arrival of the direct P phase. This zone, with an estimated crustal thickness of 19.6–21.6 km, makes up a large part of the western end of the island, mainly below Jebel Mala, Jebel Zala, and Jebel Allan, and on the coast at the SHRQ station (Figs. 2, 6a, and 8). Seven stations were located on the third E-W zone at the middle part of western Socotra between Sherubrub (SHER) on the coast and LISK station to the east (Figs. 2 and 8). It is characterized by Moho conversions that arrive within a time window of 2.67 to 3.17 s with associated depth ranges of 20.2 to 23.4 km. In our third, southernmost zone of the Central Basin, four stations constrain the crustal thickness to range between 26.4 and 28.2 km. Here the Moho conversion phase Pms delay time is of 3.5–3.7 s and multiples arrive 11.3–15.3 s after the first of P-wave arrival (Figs. 2, 6a, and 8).

The average value of the V_p/V_s ratio in the western domain of the island is ~1.75. Lower V_p/V_s ratios (1.65–1.71) are observed beneath some stations, which are located on or near granitic bodies (RUSU, DIAA and SHER) (Fig. 6b). Higher V_p/V_s ratios of 1.77–1.84 are obtained for the stations located in the Sherubrub–Balan basin (RIGI, AMAD, SHUA, HAME, MDAP, LISK and SHRQ) and also beneath DANA station near the southern coast. A high value of 1.89 is observed for the station located near the northern coast of the western domain (KADA) (Fig. 6b).

4.3. Migrated cross sections

The migrated cross sections obtained from two ~N-S profiles in the western domain of the island and two E-W profiles across the entire island are presented in Fig. 8. We utilized the IASP91 velocity-depth reference model (Kennett and Engdahl, 1991) to migrate the receiver functions from time domain to space domain, using the common conversion point (CCP) stacking technique of Dueker and Sheehan (1997) and of Zhu (2000). A bin size of 10 km width, 3 km length and 0.5 km depth is used.

The positive amplitudes, which indicate an increase of velocity with depth, are plotted in red, while negative amplitudes are shown in blue. Profile A-B, which is located at the westernmost part of the island, runs from Sherubrub on the southern coast to Kadama on the northern coast (Fig. 8b). The Moho discontinuity occurs at ~23 km beneath the southern end of profile A-B and then ascends to ~17 km beneath the northern end. The area located below KADA, RUSU and DIAA stations where the crust thins to ~16 km shows some energy placed between the surface and Moho (Yellow-Orange colors), which may indicate a rather uniform high velocity gradient extending from the surface to the Moho underneath MALA, DIAA and RUSU stations (Fig. 8a). Another feature present near the northern end of this profile is a localized upper mantle discontinuity at 43 km depth (Fig. 8a). Profile C-D, which is located ~17 km to the east of and approximately parallel to Profile A-B, extends from DANA station located on the southern coast to SHRQ station on the northern coast. The Moho depth decreases gently from ~26 km in the south (DANA and WURE) to ~20 km near the north coast (Fig. 8b).

The distribution of stations is sparser to the east along the E-W profiles. Profile E-F extends from SAYH station in the west of Ras Momi (eastern domain) to SHER station located at Sherubrub (western domain) (Fig. 8). The Moho depth is approximately equal at the two ends of the profile (~22 km) and increases to its maximum below the Haggier Mountains and plateau (Fig. 8c). Profile G-H runs parallel to the northern coast of the island from SAYH station in the west of Ras Momi (eastern domain) to MALA station located in the south of Qalansiya (western domain)(Fig. 8). Along this profile, the Moho depth increases from ~22 km at the eastern end to a ~28 km below Haggier mountains and then shallows to ~16 km at its western end below the stations located near Qalansiya (Figs. 7 and 8d). The isolated upper mantle interface at ~43 km depth below the western domain, which has been observed in the profile A-B, can also be seen on this profile. In addition we observe a constant velocity gradient that extends from the surface down to Moho below the stations located NE of Qalansiya (MALA, DIAA and RUSU) (Fig. 8d).

In the eastern part of the G-H and E-F profiles a clear positive phase is observed indicating velocity increase downward. It corresponds to a strong crustal convertor at all the eastern stations, with the exception of SAYH where it is weak and smeared. The positive phase is imaged at approximately 10 km depth and we interpret it to be mid-crustal interface between the upper and lower crust. A vertical step of about 2 km is observed near the location of HTZ and also imaged very clearly along the G-H section.

To further our understanding of the crustal structure beneath the stations in both eastern and western domains that our RFs and migrated cross sections show an intracrustal feature, we inverted the receiver function waveforms for SOCY (eastern Socotra) and DIAA (western Socotra) using the NA algorithm (Sambridge, 1999a,b). SOCY has a clear Moho conversion and multiples in addition to an intracrustal phase and thick crust (see CCP images Fig. 8c and d and RFs stacks Fig. 3a). In contrast DIAA, located in the Qalansiya Valley shows a thin crust, and the velocity increases with depth continuously rather than in discrete steps (see CCP images Fig. 8a and d). These two stations are also characterized by many events with representative RF's.

To further our understanding of the crustal structure underneath the stations in both eastern and western domains that shows an intracrustal feature in the RFs and in the migrated cross sections, we inverted the receiver function waveforms for SOCY (eastern Socotra) and DIAA (western Socotra) using the NA algorithm (Sambridge, 1999a,b). SOCY has a clear Moho conversion and multiples in addition to an intracrustal phase and thick crust (see CCP images Fig. 8c,d and RFs stacks Fig. 3a), while at DIAA, located in the Qalansiya Valley with a thin crust, the velocity increases with depth continuously rather than in discrete steps (see CCP images Fig. 8a and d). These two stations are also characterized by many events with representative RF's. Examples of inversion results are shown in Fig. 9. We obtain crustal thicknesses comparable to those obtained using the technique of Zhu and Kanamori (2000) (Figs. 4 and 5).

5. Discussion

5.1. Distinct crustal thinning on either side of a fracture zone

5.1.1. Eastern Socotra

Our crustal thickness estimates for eastern Socotra range from 27.6 km (GSFO) to 30.2 km (BIRZ) with an average of 28.6 km below the Haggier massif and 22.4–23.6 km with an average of 23.0 km to the east of the Haggier massif. Our results for the Haggier massif are very close to the crustal thickness (29.2 km) found for the southern Omani coast near Mirbat that represents the conjugate margin of the Socotra area (Tiberi et al., 2007). The crustal thinning from ~28.6 km below Haggier massif to 23 km at the easternmost part of the island occurs over ~15 km distance between HEIL/GSFO and DESH stations (Fig. 6a). Assuming a 28.6 km thick crust prior to rifting we estimate a stretching factor, β, of ~1.24. This represents a lower bound estimate for total crustal stretching since 28.6 km thickness is likely

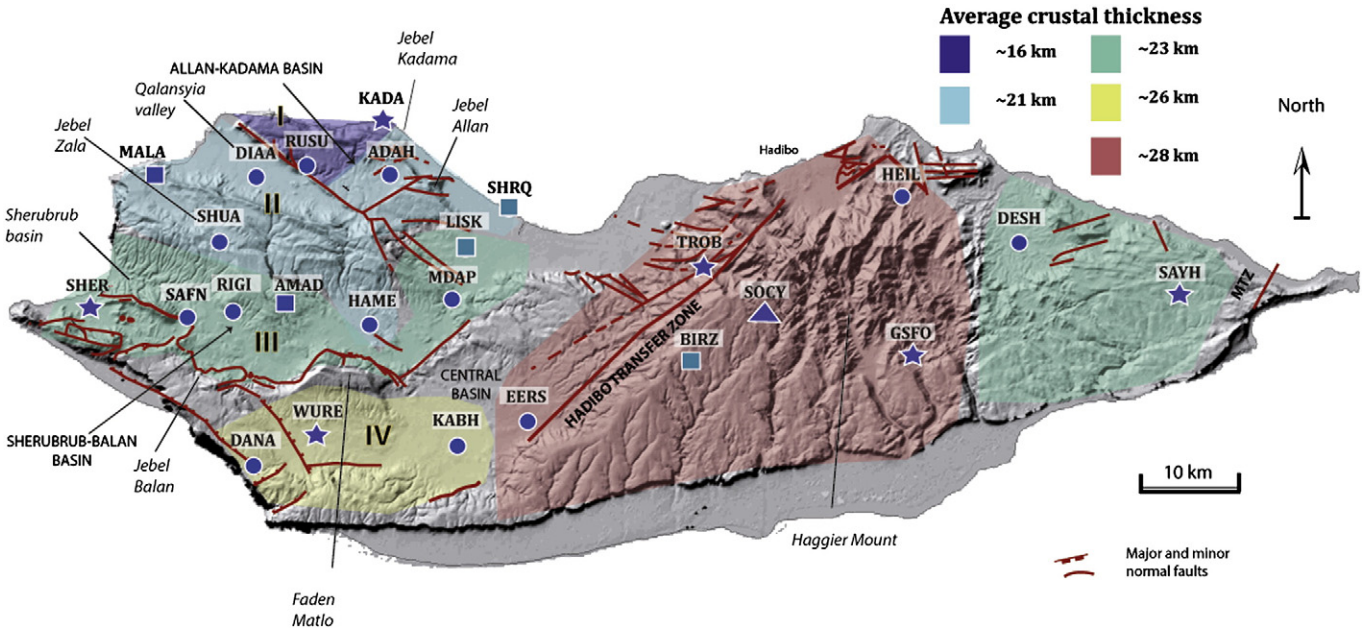

Fig. 7. Major tectonic features of Socotra and mapping of distinct zones based on average crustal thickness as listed in Table 1. Roman numbers correspond to areas described in the text with a same average crustal thickness. Red lines: major tectonic features. MTZ: Momi transfer zone; see Fig. 1 caption for the type of stations.

to be representative of crust that has been thinned during early rifting. If we assume that the unstretched crustal thickness of the Arabian platform and/or Arabian shield on the northern conjugate margin is in the range of 35–40 km (Ahmed et al., 2013; Al-Damegh et al., 2005; Al-Hashmi et al, 2011; Hansen et al., 2007; Tiberi et al., 2007) and that 23 km represents the final stretched crustal thickness, then β ranges from 1.52 to 1.74. These values are comparable to the stretching factor obtained for the northern conjugate margins studied in southern Oman and southwestern Yemen (Ahmed et al., 2013; Tiberi et al., 2007). No clear N-S change in crustal thickness and inferred degree of extension is apparent at the eastern Socotra based on the crustal thickness distribution for the stations located on the Haggier massif and close to the HTZ (ca. 28.5 $\pm$ 0.9 km). The only clear indication of crustal thinning occurs at DESH and SAYH stations towards the east in the Momi transfer zone area (Figs. 2 and 8c and d).

For all the stations located on or near the Haggier massif a clear mid-crustal interface occurs at depths between 10 and 12 km along the E-W profiles (Fig. 3). This interface appears on both profiles, but most clearly on profile G-H along the northern coast (Fig. 8d). Moreover, there is a clear vertical step in the depth to this interface from ~10 km in the east to ~12 km to the west in the vicinity of the HTZ. This interface is not imaged by the receiver functions west of the HTZ and the easternmost station SAYH. We interpret this interface to be the upper/lower crust boundary also known as the Conrad discontinuity. This discontinuity represents a sharp velocity step separating the upper crust (average V_p of 6.3 km/s) from the lower crust (average V_p of 7.0 km/s) (e.g., Ahmed et al., 2013; Mooney et al., 1985). Such an interface is a common feature in the Arabian plate (Egloff et al., 1991; Mooney et al., 1985; Stern and Johnson, 2010). Stern and Johnson (2010) suggest that it separates slower felsic upper crust from faster mafic lower crust, and may coincide with the transition from brittle to ductile deformation. A similar mid-crustal discontinuity has been reported in at least seven locations along the northern conjugate margin in southern Oman (Tiberi et al., 2007), below ASH station northern Oman (Al-Hashmi et al., 2011), and in western Yemen (Ahmed et al., 2013) towards the center of the rift axis. It disappears towards the southern edge of the syn-rift Ashawq graben on the southern coast of Oman (Tiberi et al., 2007).

Our results indicate a ~2 km vertical offset of the intracrustal discontinuity on a westward dipping plane in the vicinity of the HTZ. This feature could be related to in depth displacement across a fault zone of 10 km wide. This fault zone could belong to the HTZ which is interpreted as a dextral N050°E–N070°E transform fault (Bellahsen et al, 2013b; Denèle et al, 2012; Fournier et al, 2007; Leroy et al., 2012; Pik et al, 2013). Contrary to Fournier et al. (2007) who concluded that the HTZ was a pre-existing shallow NE-SW fracture zone within the basement, our findings of the vertical shift of Conrad discontinuity across the structure indicates that the HTZ crosscuts the Haggier massif at its western side from the surface down to the lower crust. Moreover, both the Haggier massif and HTZ are pre-existing structures inherited from early history of the margin and are less affected by the Oligo-Miocene rifting episode (Bellahsen et al, 2013b; Denele et al, 2012; Leroy et al., 2012; Pik et al, 2013).

5.1.2. Western Socotra Island

Receiver functions from stations located on the western domain of the island (Fig. 10) do not image the Conrad discontinuity. This may be caused by the crust having been strongly affected by the Oligo-Miocene rifting. Interpretation of the ENCENS cruise seismic profiles at the northern Gulf of Aden margin (Ashwaq- Salalah, Taqah and Mirbat) indicates a gradual velocity increase within the continental domain from 6.0 km/s (upper crustal velocity) to 7.0 km/s (lower crust velocity) without any velocity step (Leroy et al., 2010a). This may indicate that the extensive thinning of the crust is accompanied by removal of the upper crust and/or modification of the crustal composition. Thinning of the crust in the western domain of the island occurred by a similar mechanism of dip slip along detachment faults dividing the western domain into four different areas of uniform E-W and variable N-S crustal thickness. Leroy et al. (2012), based on recent accurate field mapping of Socotra island (Razin et al, 2010), described two complex tilted blocks where previously Fournier et al. (2007) described three tilted blocks. The first block is located along the north-west coast with the low-angle fault bounding the southern side of the ~15-km long, 5-km wide Allan–Kadama basin (Fig. 6). The two stations located in this area provide an estimated average crustal thickness of ~16.5 km, which

is the thinnest crust we observe along the southern margin of the Gulf of Aden. This result is consistent with 15–16 km thick continental crust obtained from gravity and seismic data at the southern end of a NE-SW profile along the Gulf of Aden to the west of the study area (d'Acremont et al., 2006) (Fig. 10).

The crustal thickness increases by 5 km away from the OCT over a horizontal distance of ~5 km from the stations in the Allan–Kadama basin to stations in the north of the Sherubrub–Balan basin (Fig. 7). Then it increases slightly over a distance of ~15 km from an average thickness of ~21 km in this second zone to ~23.0 km in a third zone within the Sherubrub–Balan basin. In the fourth zone in the Central basin, located at the southernmost western part of the island and furthest from the OCT, the average crustal thickness is ~26.0 km (Fig. 7). The average crustal thickness in the fourth zone is comparable to the average crustal thickness reported for the southern Omani coast in the Dhofar region (Tiberi et al., 2007) (Fig. 10). Approximately the same stretching factor, β, of 1.1 occurs between the second, third, fourth zones and Mount Haggier, but it is higher ($\beta = 1.27$) between the first and second zones. If we assume the initial crustal thickness is the same as the average for the Haggier massif (~28.6 km), and a final crustal thickness is ~16.5 km in the first block, then $\beta = 1.7$. Based upon our results for the final crustal thickness at the northwestern part of the Socotra island and assuming an initial crustal thickness of ~35–40 km (Arabian shield and platform; Al-Damegh et al., 2005; Tiberi et al., 2007; Ahmed et al., 2013) the northernmost part of Socotra island has been stretched in the NE-NNE direction by a β factor of ~2.12–2.42.

Although rifted margins show a large variability in their tectonic and sedimentary evolution related to their specific rift history and the presence of pre-existing structures, most rifted margins worldwide

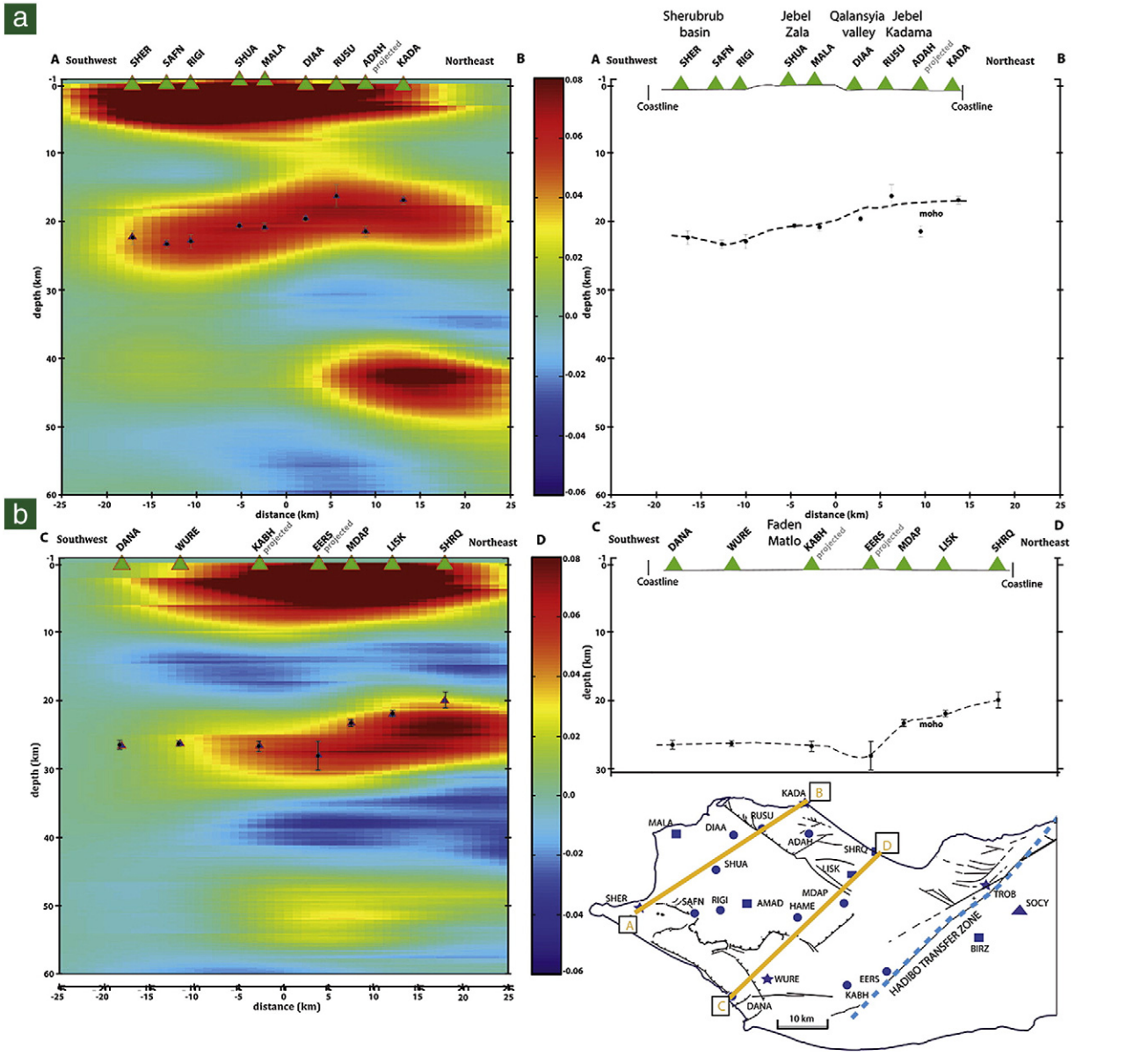

Fig. 8. Migrated cross sections with the horizontal axis corresponding to the distance in km, centered at the mid-point of the profile. The Moho depth estimated from *H–k* stacking method is plotted with the small triangles. Red color indicates velocity increase with depth, and blue color, velocity decrease with depth. Scale bar shows amplitude of positive (red) and negative (blue) polarities of arrivals. The interpretation of each cross section is presented in the right panel, HTZ: Hadibo transfer zone, MTZ: Momi transfer zone, a) SW-NE cross section at westernmost Socotra (inset for location of the cross-section A-B), b) SW-NE cross section in the middle of the western Socotra (inset for location of the cross-section C-D), c) E-W cross section along the island parallel to the southern coast (inset for location of the cross-section E-F) and d) E-W cross section along the island parallel to the northern coast (inset for location G-H).

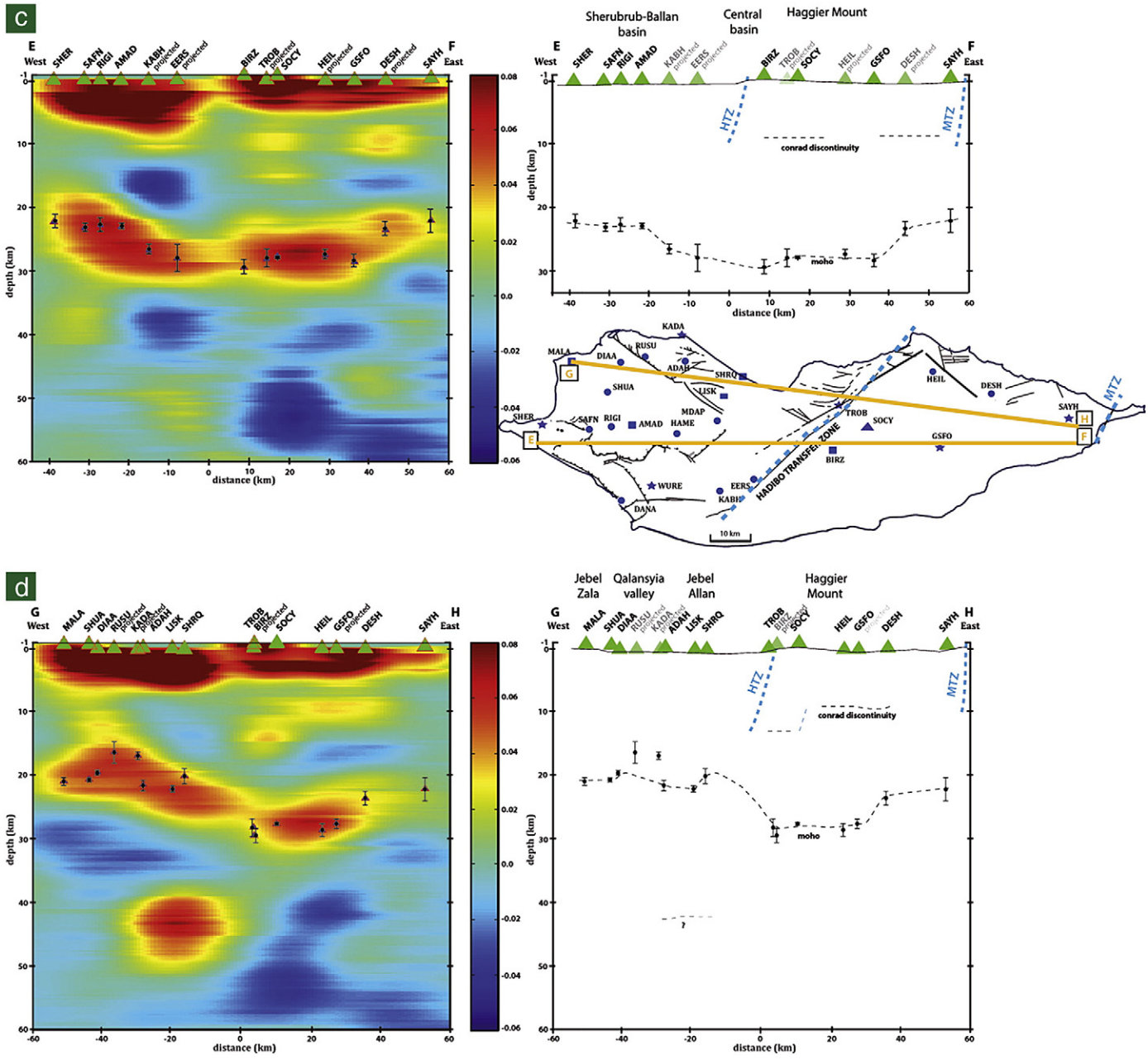

Fig. 8 (*continued*).

share a remarkably comparable large-scale architecture (Fig. 11) (Mohn et al., 2012). Based on the variations of crustal thickness and tectono-stratigraphic structure, eastern Socotra island appears to belong to the proximal margin and western Socotra to the necking zone as described by Mohn et al. (2012). The eastern domain consists of one large block tilted toward the south, with a large fault at the foot of Mount Haggier dipping toward the north on which there is at least 200 m of throw (Fig. 7 and Fig. 17 of Leroy et al., 2012). The western domain is composed of two tilted blocks with low-angle faults dipping 18° to the north. This configuration could represent the necking zone similar to that observed in the West Iberia margin (Péron-Pinvidic and Manatschal, 2008), in the offshore Aden margin (Leroy et al., 2010a) and in an outcropping margin within an orogen such as in the Alps (Mohn et al., 2012). The uniqueness of the Gulf of Aden margin is that the necking zone, which is typically hundreds of meters below water, outcrops above sea level at Socotra.

5.2. V_p/V_s ratio and crustal composition

The spatial distribution of V_p/V_s ratios correlates well with that broadly expected from the mapped rock outcrops on the island (Fig. 6b). Metamorphic basement and granitic intrusions produce low values ($1.65 \leq V_p/V_s \leq 1.71$) and sedimentary and volcanic geological units produce velocities that correspond to felsic to intermediate compositions ($1.73 \leq V_p/V_s \leq 1.84$) (Fig. 6b) (e.g. Christensen and Mooney, 1995; Hammond et al., 2011; Thompson et al., 2010). The V_p/V_s values have no obvious relationships with either crustal thickness or age of the surface rocks (Fig. 6a and b).

Five of our stations are located on or near metamorphic basement and granitic intrusions of Haggier massif, Qalansiya and Sherubrub (Figs. 2 and 6). The lowest value of 1.65 found at DIAA station, located in the Qalansiya Valley, may be related to the high silica content of paragneisses and quartzites that form the metamorphic

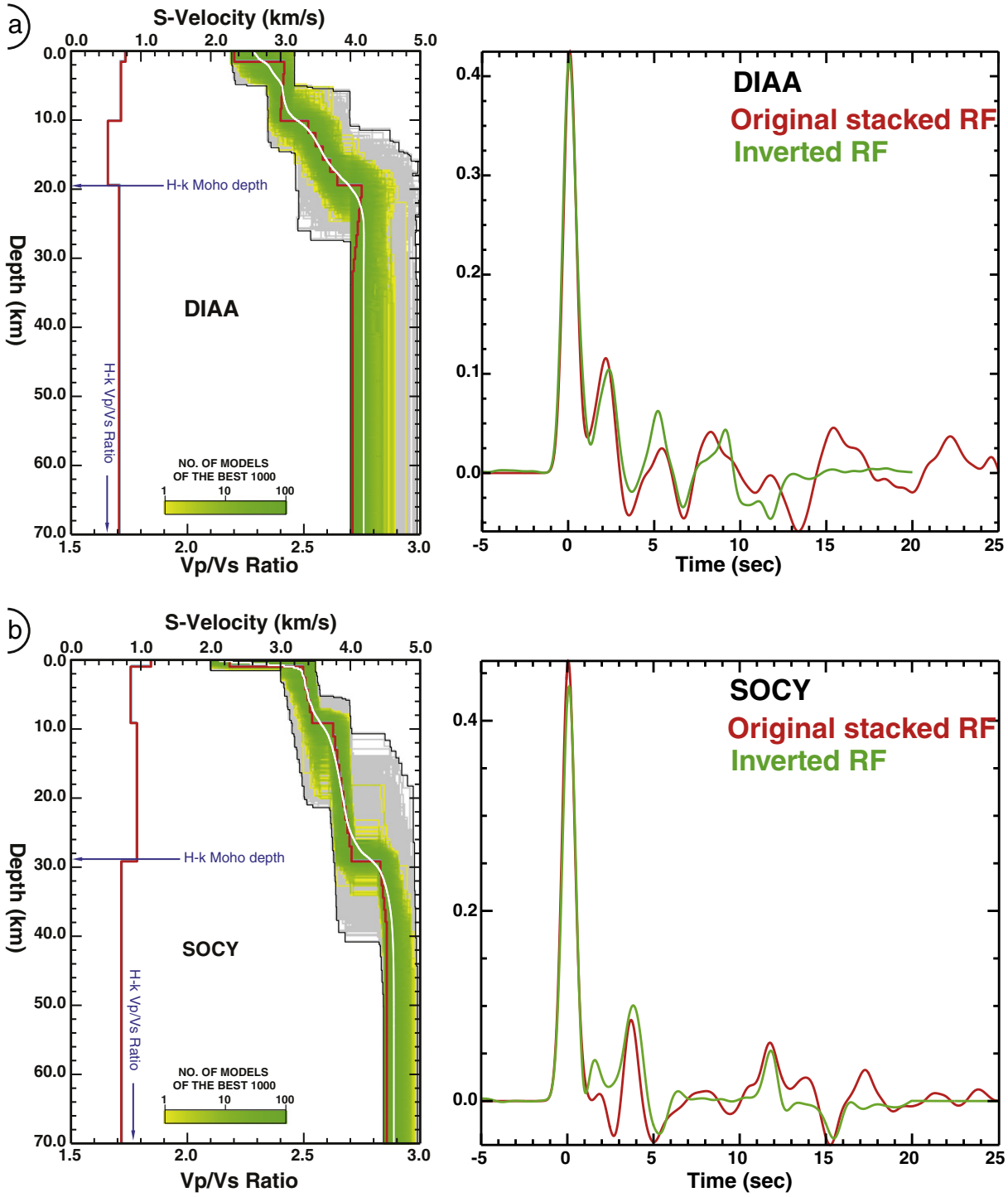

Fig. 9. a — Seismic velocity models for DIAA station (eastern Socotra) obtained from the NA method (Sambridge, 1999a) and waveform matches between the observed stacked receiver functions (red) and the predicted ones (green) based on the best models (red lines in the left diagrams). The gray area indicates the range of models employed by the algorithm. The best 1000 models are indicated in green, the red line corresponds to the best fit both for S-wave velocity and V_p/V_s ratio and the white line is the average velocity model. b — The same models for SOCY station (western Socotra).

basement (Denele et al., 2012). The other four stations (SHER, MALA, RUSU and DESH) are characterized by V_p/V_s values of 1.7–1.71, which are consistent with felsic composition of underlying rock units (Fig. 6b). On the northern conjugate margin in Dhofar–Oman very low V_p/V_s values were found at S09 station located on the metamorphic basement near Mirbat (Tiberi et al., 2007) and in western Yemen a V_p/V_s value of (~1.68) was reported for the stations located on granitic intrusions or on Precambrian quartz-rich rocks (Ahmed et al., 2013).

Results from thirteen stations, located within the sedimentary basins of the western domain of the island, are characterized by a low V_p/V_s value of ~1.73 for the stations located on a thin sedimentary cover (mostly limestone) and a higher value of ~1.83–1.84 for the stations located on a thick sedimentary cover near the middle of the basin. Similarly, in the eastern domain of Socotra, five stations located on the sedimentary cover and at or near the volcanic rocks are characterized by V_p/V_s ratios in the range 1.73–1.82. In general our finding of average V_p/V_s ratio of ~1.7 for stations located at or near silica-rich

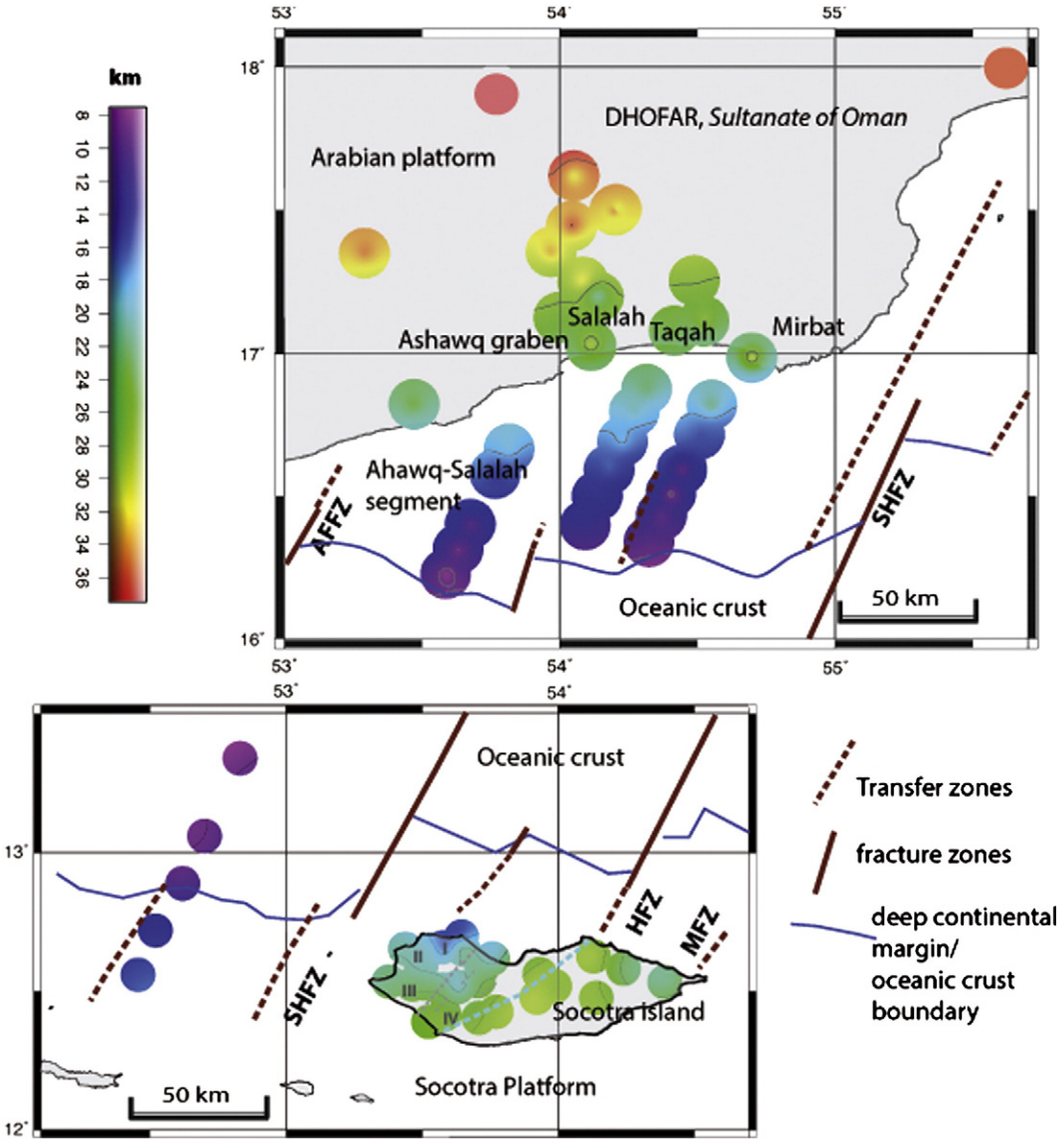

Fig. 10. Regional map showing Moho depths based on the results of this study at Socotra island and previous RF studies in Dhofar–Oman the northern conjugate margin (Al-Hashmi et al., 2011; Tiberi et al., 2007), active seismic, gravity and magnetic studies offshore to the west of Socotra (d'Acremont et al., 2006), active seismic offshore Oman — northeastern Gulf of Aden (Leroy et al., 2010a). The roman numbers at the western end of Socotra island indicate the areas with a uniform average crustal thickness as described in the result section. The blue line corresponds to the first magnetic anomaly identified (5d; 17.6 Ma; Leroy et al., 2010a). SHFZ: Socotra Hadbeen fracture zone; Alula Fartak fracture zone; MFZ: Momi fracture zone; HTZ: Hadibo fracture zone.

rock units and average V_p/V_s values of ~1.77 for stations located on the sedimentary cover are consistent with the felsic and intermediate crustal composition (Christensen, 1996; Gallacher and Bastow, 2014; De Plaen et al., 2014). Broadly our V_p/V_s ratios contrast with those at the volcanic rifted western Gulf of Aden continental margin where V_p/V_s is generally 1.8 (Ahmed et al., 2013). Our results of low V_p/V_s show that the crust has experienced minimal intrusion of mafic rock during breakup, an interpretation consistent with the lack of mafic intrusions and basaltic flows observed at the surface.

The last two stations KADA and TROB are associated with very high V_p/V_s ratios of 1.89 and 1.94 respectively (Fig. 6b). TROB station is located within the complex structure of the HTZ (Bellahsen et al., 2013b; Leroy et al., 2012; Pik et al., 2013) showing the dipping interfaces and step of the mid-crustal interface (Fig. 8d). Hence, P-wave downdip traveling multiples generated at the dipping mid-crustal interface interfere with the Moho multiples and give a poorly constrained V_p/V_s ratio which may overestimate the real value of V_p/V_s ratio beneath the station (Wang et al., 2010). In contrast, the individual receiver functions from KADA are characterized by a clear Pms converted phase and good multiples. In addition the waves approach the station in the up-dip direction that has little effect on the estimate of the V_p/V_s ratio (Wang et al., 2010). The high V_p/V_s associated with the thin crust (~16 km) may be due to a more mafic crust with magmatic intrusion near the OCT as in the northern margin (Watremez et al., 2011, 2013).

6. Conclusion

Receiver functions analyzed in Socotra allow us to map Moho depth and V_p/V_s variations along the southern Gulf of Aden margin. Variability of crustal properties yields a good correlation with tectonic structures of Socotra. Twenty-five crustal thickness (H) and V_p/V_s ratio measurements obtained by using the H–k stacking technique of Zhu and Kanamori (2000) show that:

– The crust of Socotra island is divided into distinct eastern and western domains. The eastern domain is characterized by an average of 28 km thick crust and pre-existing structures that date from the region's early pre-rift history. The western domain is

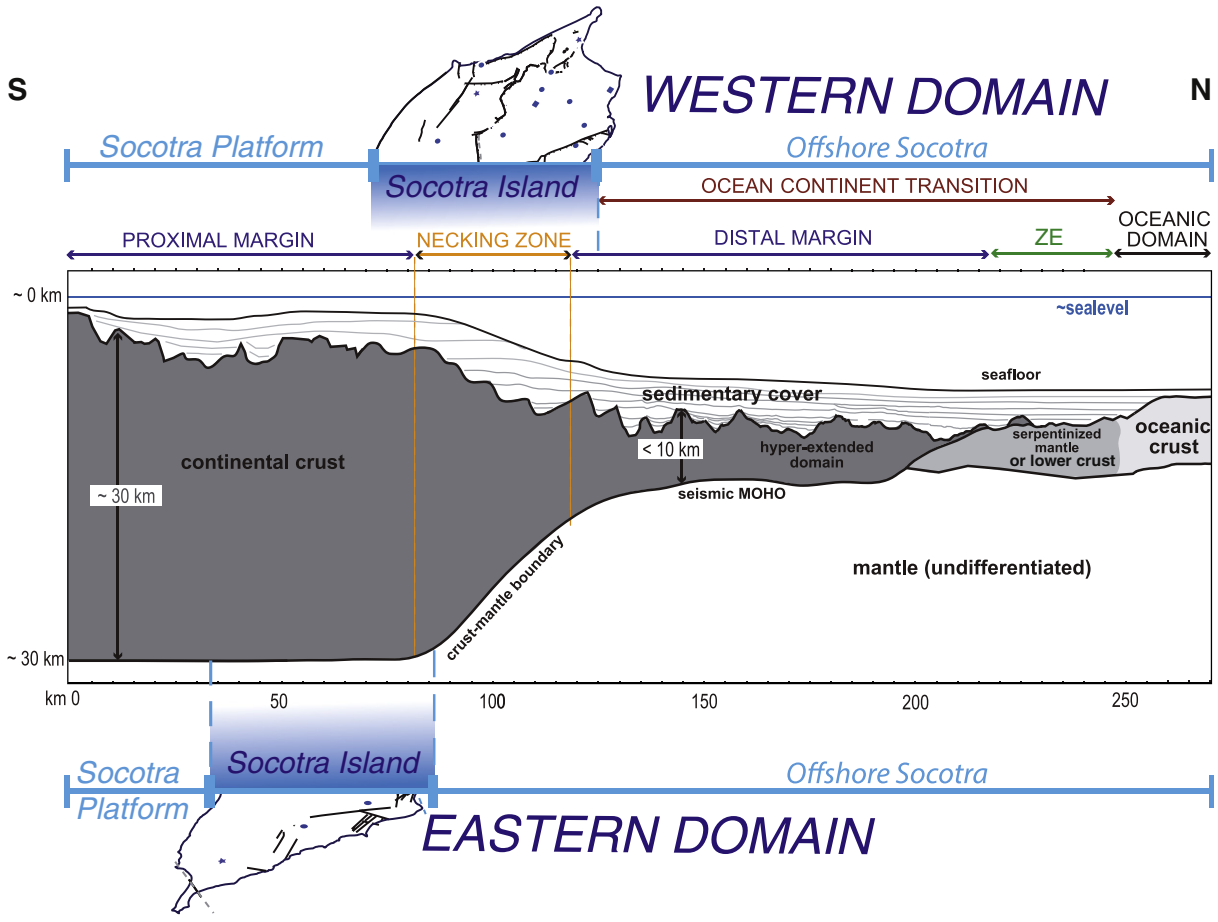

Fig. 11. Schematic transect of a magma-poor margin showing the distinct crustal domains (modified from Leroy et al., 2010a; Mohn et al., 2012) compared to distinct area of Socotra island based on crustal thickness variations. ZE: zone of exhumation.

characterized by an average of 21 km thick crust that was modified during the Oligo-Miocene rifting that led to the opening of the Gulf of Aden. The two parts are separated by the HTZ, a westward dipping plane that may extend to the lower crust.

- In the western domain, rifting resulted in progressive crustal thinning from 26 km in the south to 16.4 km in the north of the island. Four structurally distinct E-W trending areas of average crustal thicknesses of 16.5, 21, 23 and 26 km are defined.
- Assuming the initial crustal thickness of 28.6 km, the maximum currently observed below Socotra, and thinnest crustal thickness of 16.5 km, we estimate a lower bound stretching factor of 1.7. However, a higher stretching factor in the range of ~2.1–2.4 is obtained by assuming the initial crustal thickness more compatible with an undeformed continent such as that found for the Arabian plate (35 km).
- An uppermost mantle reflector beneath the anomalously thin crust in the northernmost part of the island has been imaged by our computed receiver functions, but evidence for removal of lower crust and/or underplating could not be assessed with our dataset.
- We computed V_p/V_s to vary between 1.7 and 1.77 at the majority of the stations. This is consistent with a felsic to intermediate crust beneath the stations located at the regions of granite intrusion or at sedimentary basin. The highest V_p/V_s ratios ranging between 1.78 and 1.84 are mainly associated with sediments. Broadly, the low V_p/V_s ratios are consistent with no or very low volume intrusion of mafic rock into the OCT during breakup, and therefore suggests that magma intrusion did not accommodate significant extension during the breakup of the eastern Gulf of Aden.
- From our observations we propose that the western part of Socotra corresponds to the necking zone of a classic magma-poor continental margin, while the eastern part corresponds to the proximal domain.

Acknowledgments

We gratefully acknowledge Alex Brisbourne, Victoria Lane and David Hawthorn (NERC Seis-UK equipment pool), the French Embassy in Yemen (J.G. Sarkis, J. Dechezlepretre and C. Bousquet), local governers and the people of the Yemen governerates for their help during the field work. We deeply thank Dr. I. Al Ganad from GSMRB during the deployment. We thank C. Tiberi, J. Vergne, and G. Hetenyi for providing software. The work was funded by the Agency National de la Recherche ANR-07-BLAN-0135 YOCMAL project and Rift2ridge project, CNRS-INSU-PICS Yemen, GSMRB Yemen and Actions Marges. The facilities of SEIS-UK are supported by the Natural Environment Research Council (NERC) under Agreement R8/H10/64. D.K. is supported by NERC grant NE/L013932/1.

Appendix A. Supplementary data

Supplementary data to this article can be found online at http://dx.doi.org/10.1016/j.tecto.2014.10.014.

References

Ahmed, A., Tiberi, C., Leroy, S., Stuart, G.W., Keir, D., Sholan, J., Khanbari, K., Al-Ganad, I., Basuyau, C., 2013. Crustal structure of the rifted volcanic margins and uplifted plateau of Western Yemen from receiver function analysis. Geophys. J. Int. http://dx.doi.org/10.1093/gji/ggt072.

Al-Amri, A., 1998. The crustal structure of the Western Arabian platform from the spectral analysis of long-period P-wave amplitude ratios. Tectonophysics 290, 271–283.

Al-Amri, A., 1999. The crustal and upper-mantle structure of the interior Arabian platform. Geophys. J. Int. 136, 421–430.

Al-Damegh, K., Sandoval, E., Brazangi, M., 2005. Crustal structure of the Arabian plate: new constraints from the analysis of teleseismic receiver functions. Earth Planet. Sci. Lett. 231, 177–196.

Al-Hashmi, S., Gok, R., Al-Toubi, K., Al-Shijbi, Y., El-Hussain, I., Rodgers, A.J., 2011. Seismic velocity structure at the southeastern margin of the Arabian Peninsula. Geophys. J. Int. http://dx.doi.org/10.1111/j.1365-246X.2011.05067.x.

Ali, M.Y., Watts, A.B., 2013. Subsidence history, crustal structure, and evolution of the Somaliland-Yemen conjugate margin. J. Geophys. Res. Solid Earth 118, 1638–1649.

Al-Lazki, A., Ebinger, C., Kendall, M., Helffrich, G., Leroy, S., Tiberi, C., Stuart, G., Al-Toobi, K., 2012. Upper mantle anisotropy of southeast Arabia passive margin [Gulf of Aden northern conjugate margin], Oman. Arab. J. Geosci. 5 (5), 925–934. http://dx.doi.org/10.1007/s12517-011-0477-2.

Autin, J., Leroy, S., Beslier, M.O., d'Acremont,, E., Razin, P., Ribodetti, A., Bellahsen, N., Robin, C., Al-Toubi, K., 2010a. Continental break-up history of a deep magma-poor margin from seismic reflection data (northeastern Gulf of Aden margin, offshore Oman). Geophys. J. Int. 180, 501–519.

Autin, J., Bellahsen, N., Husson, L., Beslier, M.O., Leroy, S., d'Acremont, E., 2010b. Analogue models of oblique rifting in a cold lithosphere. Tectonics 29, TC6016.

Bache, F., Leroy, S., Baurion, C., Robinet, J., Gorini, C., Lucazeau, F., Razin, P., d'Acremont,, E., Al-Toubi, K., 2011. Post-rift uplift of the Dhofar margin (Gulf of Aden). Terra Nova 23, 11–18. http://dx.doi.org/10.1111/j.1365-3121.2010.00975.x.

Basuyau, C., Tiberi, C., Leroy, S., Stuart, G., Al-Lazki, A., Al-Toubi, K., Ebinger, C., 2010. Evidence of partial melting beneath a continental margin: case of Dhofar, in the Northeast Gulf of Aden (Sultanante of Oman). Geophys. J. Int. 180, 520–534.

Bellahsen, N., Fournier, M., d'Acremont, E., Leroy, S., Daniel, J.M., 2006. Fault reactivation and rift localization: northeastern Gulf of Aden margin. Tectonics 25, TC1007. http://dx.doi.org/10.1029/2004TC001626.

Bellahsen, N., Husson, L., Autin, J., Leroy, S., d'Acremont, E., 2013a. The effect of thermal weakening and buoyancy forces on rift localization: field evidences from the Gulf of Aden oblique rifting. Tectonophysics 607, 80–97.

Bellahsen, N., Leroy, S., Autin, J., Razin, P., d'Acremont, E., Sloan, H., Pik, R., Ahmed, A., Khanbari, K., 2013b. Pre-existing oblique transfer zones and transfer/transform relationships in continental margins: new insights from the southeastern Gulf of Aden, Socotra Island Yemen. Tectonophysics 607, 32–50.

Beydoun, Z.R., Bichan, H.R., 1969. The geology of Socotra Island, Gulf of Aden. Quat. J. 125, 413–446.

Birse, A.C.R., Bott, W.F., Morrison, J., Samuel, M.A., 1997. The Mesozoic and early Tertiary tectonic evolution of the Socotra area, eastern Gulf of Aden, Yemen. Mar. Pet. Geol. 14, 675–684.

Brown, B.C., 1931. The geology of North-Eastern British Somaliland. Q. J. Geol. Soc. Lond. 87, 259–280.

Brune, S., Autin, J., 2013. The rift to break-up evolution of the Gulf of Aden: insights from 3D numerical lithospheric-scale modelling. Tectonophysics 607, 65–79.

Chang, S., Van der Lee, S., 2011. Mantle plumes and associated flow beneath Arabia and East Africa. Earth Planet. Sci. Lett. 302 (3–4), 448–454.

Christensen, N.I., 1996. Poisson's ratio and crustal seismology. J. Geophys. Res. 101, 3139–3156. http://dx.doi.org/10.1029/95JB03446.

Christensen, N.I., Mooney, W.D., 1995. Seismic velocity structure and composition of the continental crust: a global view. J. Geophys. Res. 100, 9761–9788.

Corbeau, J., Rolandone, F., Leroy, S., Al-Lazki, A., Stork, A., Keir, D., Stuart, G., Doubre, C., Vergne, J., Ahmed, A., Khanbari, K., 2014. Uppermost mantle velocity from Pn tomography in the Gulf of Aden. Geosphere http://dx.doi.org/10.1130/ges01052.1.

d'Acremont,, E., Leroy, S., Beslier, M.O., Bellahsen, N., Fournier, M., Robin, C., Maia, M., Gente, P., 2005. Structure and evolution of the eastern Gulf of Aden conjugate margins from seismic reflection data. Geophys. J. Int. 160, 869–890.

d'Acremont,, E., Leroy, S., Maia, M., Patriat, P., Beslier, M.O., Bellahsen, N., Fournier, M., Gente, P., 2006. Structure and evolution of the eastern Gulf of Aden: insights from magnetic and gravity data (Encens- Sheba/MD117 cruise). Geophys. J. Int. 165, 786–803.

d'Acremont,, E., Leroy, S., Maia, M., Gente, P., Autin, J., 2010. Volcanism, jump and propagation on the Sheba Ridge, eastern Gulf of Aden: segmentation evolution and implications for accretion processes. Geophys. J. Int. 180, 535–551.

De Plaen, R.S.M., Bastow, I.D., Chambers, E.L., Keir, D., Gallacher, R., 2014. The development of magmatism along the Cameroon Volcanic Line: evidence from seismicity and seismic anisotropy. J. Geophys. Res. 119, 4233–4252.

Denèle, Y., Leroy, S., Pelleter, E., Pik, R., Talbot, J.Y., Khanbari, K., 2012. The Cryogenian juvenile Arc formation and successive high-K calc-alkaline plutons intrusion of Socotra Island Yemen. Arab. J. Geosci. 5 (5), 903–924. http://dx.doi.org/10.1007/s12517-011-0476-3.

Dueker, K.G., Sheehan, A.F., 1997. Mantle discontinuity structure from midpoint stacks of converted P to S waves across the Yellowstone hotspot track. J. Geophys. Res. 102, 8313.

Efron, B., Tibshirani, R., 1986. The Bootstrap Method for standard errors, confidence intervals, and other measures of statistical accuracy. Stat. Sci. 1 (1), 1–35.

Egloff, F., Rihm, R., Makris, J., Izzeldin, Y.A., Bobsien, M., Meier, K., Junge, I., Noman, T., Warsi, W., 1991. Contrasting structural styles of the eastern and westernmargins of the southern Red Sea: the 1988 SONNE experiment. In: Makris, J., Mohr, P., Rihm, R. (Eds.), Red Sea: Birth and Early History of a New Oceanic Basin. Tectonophysics 198, pp. 329–353.

Fantozzi, P.L., 1996. Transition from continental to oceanic rifting in the Gulf of Aden: structural evidence from field mapping in Somalia and Yemen. Tectonophysics 259, 285–311. http://dx.doi.org/10.1016/0040-1951(95) 00208-1.

Fantozzi, P.L., Sgavetti, M., 1998. Tectonic and sedimentary evolution of the eastern Gulf of Aden continental margins: new structural and stratigraphic data from Somalia and Yemen. In: Purser, B.H., Bosence, D.W.J. (Eds.), Sedimentation and Tectonics of Rift Basins: Red Sea-Gulf of Aden. CRC Press, Boca Raton, FL, pp. 56–76.

Fournier, M., Huchon, P., Khanbari, K., Leroy, S., 2007. Asymmetry and segmentation of passive margin in Socotra, Eastern Gulf of Aden, controlled by detachment faults? Geochem. Geophys. Geosyst. 8 (3), Q03013 (03010.01029/02006GC001318).

Fournier, M., Chamot-Rooke, N., Petit, C., Huchon, P., Al-Kathiri, A., Audin, L., Beslier, M.O., d'Acremont,, E., Fabbri, O., Fleury, J.M., Khanbari, K., Lepvrier, C., Leroy, S., Maillot, B., Merkouriev, S., 2010. Arabia–Somalia plate kinematics, evolution of the Aden–Owen–Carlsberg triple junction, and opening of the Gulf of Aden. J. Geophys. Res. 115 (B4), B04102. http://dx.doi.org/10.1029/2008jb006257.

Franke, D., 2013. Rifting, lithosphere breakup and volcanism: comparison of magma-poor and volcanic rifted margins. Mar. Pet. Geol. 43, 63–87.

Gallacher, R., Bastow, I.D., 2014. The development of magmatism along the Cameroon Volcanic Line: evidence from teleseismic receiver functions. Tectonics 31, TC3018. http://dx.doi.org/10.1029/2011TC003028.

Granath, J.W., 2001. The Nogal rift of northern Somalia: Gulf of Aden. Reactivation of a Mesozoic rift. In: Ziegler, P.A., et al. (Eds.), Peri-Tethys memoir 6: Peri-Tethyan rifts/Wrench basins and passive margins. Mem. Mus. Nat. Hist. 186, pp. 511–552.

Hammond, J.O.S., Kendall, J.-M., Stuart, G.W., Keir, D., Ebinger, C., Ayele, A., Belachew, M., 2011. The nature of the crust beneath the Afar triple junction: evidence from receiver functions. Geochem. Geophys. Geosyst. 12, Q12004. http://dx.doi.org/10.1029/2011GC003738.

Hansen, S.E., Rodgers, A.J., Schwartz, S.Y., Al-Amri, A.M.S., 2007. Imaging ruptured lithosphere beneath the Red Sea and Arabian Peninsula. Earth Planet. Sci. Lett. 259, 256–265.

Huchon, P., Khanbari, K., 2003. Rotation of the syn-rift stress field of the northern Gulf of Aden margin Yemen. Tectonophysics 364, 147–166.

Kennett, B.L.N., Engdahl, E.R., 1991. Traveltimes for global earthquakelocation and phase identification. Geophys. J. Int. 122, 429–465.

Korostelev, F., Basuyau, C., Leroy, S., Tiberi, C., Ahmed, A., Keir, D., Stuart, G., Rolandone, F., Al Ganad, I., Khanbari, K., Boschi, L., 2014. Crustal and upper mantle structure beneath south-western margin of the Arabian Peninsula from teleseismic tomography. Gcubed http://dx.doi.org/10.1002/2014GC005316.

Langston, C.A., 1977. Corvallis, Oregon, crustal and upper mantle structure from teleseismic P and S waves. Bull. Seismol. Soc. Am. 67, 713–724.

Langston, C.A., 1979. Structure under Mount Rainier, Washington, inferred from teleseismic body waves. J. Geophys. Res. 84, 4749–4762.

Laughton, A.S., Whitmarsh, R.B., Jones, M.T., 1970. The evolution of the Gulf of Aden. Philos. Trans. R. Soc. Lond. 267 (Ser. A), 227–266.

Leroy, S., Gente, P., Fournier, M., d'Acremont,, E., Patriat, P., Beslier, M.-O., Bellahsen, N., Maia, M., Blais, A., Perrot, J., Al-Kathiri, A., Merkouriev, S., Fleury, J.-M., Ruellan, P.-Y., Lepvrier, C., Huchon, P., 2004. From rifting to spreading in the eastern Gulf of Aden: a geophysical survey of a young oceanic basin from margin to margin. Terra Nova 16, 185–192.

Leroy, S., Lucazeau, F., d'Acremont,, E., Watremez, L., Autin, J., Rouzo, S., Bellahsen, N., Tiberi, C., Ebinger, C., Beslier, M.-O., Perrot, J., Razin, P., Rolandone, F., Sloan, H., Stuart, G., Al-Lazki, A., Al-Toubi, K., Bache, F., Bonneville, A., Goutorbe, B., Huchon, P., Unternehr, P., Khanbari, K., 2010a. Contrasted styles of rifting in the eastern Gulf of Aden: a combined wide-angle MCS and Heat flow survey. Geochem. Geophys. Geosyst. http://dx.doi.org/10.1029/2009GC002963.

Leroy, S., d'Acremont,, E., Tiberi, C., Basuyau, C., Autin, J., Lucazeau, F., 2010b. Recent off-axis volcanism in the eastern Gulf of Aden: implications for plume-ridge interactions. Earth Planet. Sci. Lett. 140–153 http://dx.doi.org/10.1016/j.epsl.2010.02.036, 293.

Leroy, S., Razin, P., Autin, J., Bache, F., d'Acremont, E., Watremez, L., Robinet, J., Baurion, C., Denèle, Y., Bellahsen, N., Lucazeau, F., Rolandone, F., Rouzo, S., Serra Kiel, J., Robin, C., et al., 2012. From rifting to oceanic spreading in the Gulf of Aden: a synthesis. Arab. J. Geosci. http://dx.doi.org/10.1007/s12517-011-0475-4.

Ligorria, J., Ammon, G., 1999. Iterative deconvolution and receiver functions estimation. Bull. Seismol. Soc. Am. 89, 1395–1400.

Lucazeau, F., Leroy, S., Bonneville, A., Goutorbe, B., Rolandone, F., d'Acremont, E., Watremez, L., Düsünur,, D., Tuchais, P., Huchon, P., Bellahsen, N., Al-Toubi, K., 2008. Persistent thermal activity at the Eastern Gulf of Aden after continental break-up. Nat. Geosci. 854–858 http://dx.doi.org/10.1038/ngeo359.

Lucazeau, F., Leroy, S., Autin, J., Bonneville, A., Goutorbe, B., Rolandone, F., d'Acremont,, E., Watremez, L., Düsünur,, D., Huchon, P., 2009. Post-rift volcanism and high heat-flow at the ocean–continent transition of the Gulf of Aden. Terra Nova 21 (4), 285–292.

Lucazeau, F., Leroy, S., Rolandone, F., d'Acremont, E., Watremez, L., Bonneville, A., Goutorbe, B., Düsünur,, D., 2010. Heat-flow and hydrothermal circulations at the ocean–continent transition of the Eastern Gulf of Aden. Earth Planet. Sci. Lett. 295 (3–4), 554–570. http://dx.doi.org/10.1016/j.epsl.2010.04.039.

Menzies, M., et al., 1992. The timing of crustal magmatism, uplift and crustal extension-preliminary observations from Yemen. In: Storey, B., et al. (Eds.), Magmatism and the Causes of Continental Break-up. Geol. Soc. Lond. Spec. Publ. 68, pp. 293–304.

Menzies, M., Gallagher, K., Yelland, A., Hurford, A.J., 1997. Volcanic and nonvolcanic rifted margins of the Red Sea and Gulf of Aden; crustal cooling and margin evolution in Yemen. Geochim. Cosmochim. Acta 61 (12), 2511–2527.

Mohn, G., Manatschal, G., Beltrando, M., Masini, E., Kusznir, N., 2012. Necking of continental crust in magma-poor rifted margins: evidence from the fossil Alpine Tethys margins. Tectonics 31, TC1012. http://dx.doi.org/10.1029/2011TC002961.

Mooney, W.D., Gettings, M.E., Blank, H.R., Healey, J.H., 1985. Saudi Arabian seismic refraction profile: a traveltime interpretation of crustal and upper mantle structure. Tectonophysics 111, 173–246.

Morrison, J., Birse, A., Samuel, M.A., Richardson, S.M., Harbury, N., Bott, W.F., 1997. The Cretaceous sequence stratigraphy of the Socotran platform, the Republic of Yemen. Mar. Pet. Geol. 14, 685–699.

Owens, T.J., Zandt, G., Taylor, S.R., 1984. Seismic evidence for an ancient rift beneath the Cumberland Plateau, Tennessee: a detailed analysis of broadband teleseismic P-waveforms. J. Geophys. Res. 89, 7783–7795.
Péron-Pinvidic, G., Manatschal, G., 2008. The final rifting evolution at deep magma-poor passive margins from Iberia-Newfoundland: a new point of view. Int. J. Earth Sci. http://dx.doi.org/10.1007/s00531-00008-00337-00539.
Pik, R., Bellahsen, N., Leroy, S., Denèle, Y., Razin, P., Ahmed, A., Khanbari, K., 2013. Structural control of basement 1 denudation in the course of rift development revealed by low-temperature (U–Th–Sm)/He thermochronology of the Socotra Island basement — southern Gulf of Aden margin. Tectonophysics 607, 17–31.
Platel, J.P., Roger, J., 1989. Evolution dynamique du Dhofar (Sultanat d'Oman) pendant le Crétacé et le Tertiaire en relation avec l'ouverture du Golfe d'Aden. Bull. Soc. Geol. Fr. 8 (2), 253–263.
Platel, J. P., Roger, J., Peters, T. J., Mercolli, I., Kramers, J. D. and Le Me´tour, J., 1992. Geological map of Salalah, Sultanate of Oman, sheet NE 40-09, scale 1:250,000. Minist. of Pet. and Miner., Dir. Gen. of Miner., Muscat, Sultanate of Oman.
Razin, P., Robin, C., Serra Kiel, J., Bellahsen, N., Leroy, S., Grelaud, C., Robinet, J., 2010. Cenozoic evolution of Socotra Island in relation with the opening of the Gulf of Aden. EGU, Vienna.
Robinet, J., Razin, P., Serra-Kiel, J., Gallardo-Garcia, A., Leroy, S., Roger, J., Grelaud, C., 2013. The Paleogene pre-rift to syn-rift succession in the Dhofar margin (northeastern Gulf of Aden): stratigraphy and depositional environments. Tectonophysics 607, 1–16.
Rolandone, F., Lucazeau, F., Leroy, S., Mareschal, J.C., Jorant, R., Goutorbe, B., Bouquerel, H., 2013. New heat flow measurements in Oman and the thermal state of the Arabian shield and platform. Tectonophysics 589, 77–89. http://dx.doi.org/10.1016/j.tecto.2012.12.034.
Sambridge, M., 1999a. Geophysical inversion with a neighbourhood algorithm-I Searching a parameter space. Geophys. J. Int. 138, 479–494.
Sambridge, M., 1999b. Geophysical inversion with a neighbourhood algorithm—II Appraising the ensemble. Geophys. J. Int. 138, 727–746.
Samuel, M.A., Harbury, N., Bott, R., Thabet, A.M., 1997. Field observations from the Socotran platform: their interpretation and correlation to Southern Oman. Marine and Petroleum Geology 14, 661–673.
Shibutani, T., Sambridge, M., Kennett, B., 1996. Genetic algorithm inversion for receiver functions with application to crust and uppermost mantle structure beneath Eastern Australia. Geophys. Res. Lett. 23 (14). http://dx.doi.org/10.1029/96GL01671 (issn: 0094-8276).
Stein, C.A., Cochran, J.R., 1985. The transition between the Sheba ridge and the Owen basin: rifting of old oceanic lithosphere. Geophys. J. R. Astron. Soc. 81, 47–74.
Stern, R.J., Johnson, P., 2010. Continental lithosphere of the Arabian Plate: a geologic, petrologic, and geophysical synthesis. Earth Sci. Rev. 101, 29–67.
Thompson, D.A., Bastow, I.D., Helffrich, G., Kendall, J.-M., Wookey, J., Snyder, D.B., Eaton, D.W., 2010. Precambrian crustal evolution: seismic constraints from the Canadian shield. Earth Planet. Sci. Lett. 297, 655–666. http://dx.doi.org/10.1016/j.epsl.2010.07.021.
Tiberi, C., Leroy, S., d'Acremont,, E., Bellahsen, N., Ebinger, C., Al-Lazki, A., Pointu, A., 2007. Crustal geometry of the northeastern Gulf of Aden passive margin: localization of the deformation inferred from receiver function analysis. Geophys. J. Int. 168, 1247–1260. http://dx.doi.org/10.1111/j.1365-246X.2006.03294.x.
Vinnik, L.P., 1977. Detection of waves converted from P to SV in the mantle. Phys. Earth Planet. Inter. 15, 39–45.
Wang, P., Wang, L., Mi, N., Liu, J., Li, H., Yu, D., Xu, M., Wang, X., Guo, Z., 2010. Crustal thickness and average Vp /Vs ratio variations in southwest Yunnan, China, from teleseismic receiver functions. J. Geophys. Res. 115, B11308. http://dx.doi.org/10.1029/2009JB006651.
Watremez, L., Leroy, S., Rouzo, S., d'Acremont,, E., Unternehr, P., Ebinger, C., Lucazeau, F., Al Lazki, A., 2011. The crustal structure of the northeastern Gulf of Aden continental margin: insights from wide-angle seismic data. Geophys. J. Int. 184, 575–594.
Watremez, L., Burov, E., d'Acremont,, E., Leroy, S., Huet, B., Le Pourhiet, L., Bellahsen, N., 2013. Buoyancy and localizing properties of continental mantle lithosphere: insights from thermomechanical models of the eastern Gulf of Aden. G3 14, 2800–2817.
Whitmarsh, R.B., Manatschal, G., Minshull, T.A., 2001. Evolution of magma-poor continental margins from rifting to seafloor spreading. Nature 413, 150–154. http://dx.doi.org/10.1038/35093085.
Zandt, G., Myers, S., Wallace, T., 1995. Crust and mantle structure across the Basin and Range-Colorado Plateau boundary at 37°N latitude and implications for Cenozoic extensional mechanism. J. Geophys. Res. 100, 10 529–10 548.
Zhu, L., 2000. Crustal structure across the San Andreas Fault, Southern California from teleseismic converted waves. Earth Planet. Sci. Lett. 179, 183–190.
Zhu, L., Kanamori, H., 2000. Moho depth variation in Southern California from teleseimic receiver function. J. Geophys. Res. 105, 2969–2980.